Correlative light and electron microscopy : strategies and applications

Driel, L.F. van

Chapter 1

Introduction

This chapter is partly modified from:

Valentijn J.A.; van Driel L.F.; Jansen K.A.; Valentijn K.M.; Koster A.J. Towards a 3D View of Cellular Architecture: Correlative Light Microscopy and Electron Tomography. Book chapter in: Reiner Salzer. *Biomedical Imaging: Principles and Applications.* Wiley, 2010.

The present thesis reports on newly developed tools and strategies for correlative light and electron microscopy, and their application to cell biology research aimed at furthering our understanding of the structure-functional mechanisms of varying current biological applications. Accordingly, this Introduction consists of two main parts: the first one will discuss past and present strategies for correlative light and electron microscopy (CLEM) as an introduction to the subsequent chapters in this thesis, all of which will describe new developments and applications in the field; the second one will elaborate on the rationale behind the biological applications that were undertaken.

1.1. Correlative Microscopy

The term 'correlative microscopy' is employed in the biomedical literature to designate any combination of two or more microscopic techniques applied to the same region in a biological specimen. The purpose of correlative microscopy is to obtain complementary data, each imaging modality providing different information, on the specimen that is under investigation. Correlative light and electron microscopy (CLEM) is by far the most widespread form of correlative microscopy.

CLEM makes use of the fact that imaging with photons on the one hand, and electrons on the other hand, each offers specific advantages over one another. For instance, the low-magnification range inherent to light microscopy (LM) is particularly well-suited for the rapid scanning of large and heterogeneous sample areas, while the high magnification and -resolution that can be achieved by electron microscopy (EM) allows for the subsequent zooming in on selected areas of interest to obtain ultrastructural detail. A further advantage of LM is that it can be used to study dynamic processes, up to the molecular level, in living cells and tissues. The recent surge in live cell imaging research has catalyzed a renewed interest in CLEM methodologies, as the interpretation of the dynamic processes observed by LM often requires high-resolution information from EM data. CLEM is also gaining in momentum in the field of cryo-electron microscopy where the low contrast conditions and low electron dose requirements put a constraint on the detection efficacy.

Current CLEM procedures face a number of challenges. Firstly, sample preparation methods for LM and EM can be quite divergent due to different requirements for preservation, embedding, sectioning, and counterstaining. Therefore, alternative sample preparation protocols need to be devised that are suitable for both LM and EM. Secondly, CLEM often requires the correlated localization of specific molecules in cells or tissues, for which specialized detection systems need to be developed. Standard detection methods are based on tagging of molecules either with fluorochromes for LM, or with gold particles for EM, whereas some CLEM applications require a

tag to be visible in both modalities. Thirdly, the transition from imaging by LM to EM may involve handling and additional processing of samples, which can lead to changes in orientation and morphology of the sample. This in turn can hamper the finding back of, and correlation with previously established areas of interest.

1.1.1. Historical Perspective

When Porter, Claude and Fullam published in their 1945 landmark paper the earliest transmission electron-microscopic images of an intact cell, describing for the first time the endoplasmic reticulum, they made a side-by-side comparison with light-microscopic images (Porter et al., 1945). Although they did not perform genuine CLEM – the light and electron micrographs were not taken from the same cells – the authors clearly felt the need to correlate their electron-microscopic observations with the more familiar light-microscopic data as a means to validate their novel findings. Thus, in a sense, CLEM is as old as the earliest applications of EM to biological samples. In the ensuing 1950s-80s numerous 'correlated light and electron microscopic' studies were published based on the same concept of comparing structures observed by LM with similar structures visualized by EM. True CLEM emerged in the early 1970s, and culminated in the 1980s with the publication of a dedicated book in the authoritative Hayat series on EM techniques (Hayat, 1987), and with the development of instrumentation such as a combined instrument for LM and scanning EM (Wouters and Koerten, 1982), and the commercial LEM 2000 (Akashi Seisakusho Ltd., Tokyo, Japan) for LM and transmission EM (TEM). Interestingly, among the first genuine CLEM applications were studies that combined TEM with live cell imaging (Buckley, 1971), the latter boosting again the recent revival of CLEM. Neuroanatomy was another field of research that pioneered CLEM techniques to facilitate sampling of central nervous tissue for TEM (Hollander, 1970).

The 1990s saw a steady decrease in the use of EM for cell biology studies (Geuze, 1999). Several factors were responsible for this decline. Firstly, the genomics era was in full bloom, and the inherent emphasis on functional/mechanistic studies overshadowed the static images and descriptive data that EM produced. Secondly, there had been major developments in light microscopy, the most important of which was the introduction of 'turnkey' systems for confocal laser scanning microscopy. These systems offered improved resolution up to the subcellular level, while requiring less investment, infrastructure, and expertise than a typical EM setup. Last but not least, the discovery of green fluorescent protein (GFP) and the demonstration that it could be used to tag proteins genetically, stirred a revolution in biomedical research as it allowed for the tracking of specific proteins in living cells by means of fluorescence microscopy.

In the present post-genomics climate, EM is coming back with a vengeance. Despite the dip in EM-based research during the previous decade, the development of novel EM technologies moved forward at a steady pace, resulting in several breakthrough applications. Among them are electron tomography and cryo-electron tomography, which are techniques for high-resolution 3D visualization and which are gradually becoming mainstream tools in structural molecular biology. As will be discussed in more detail below, (cryo-)electron tomography is often hampered by the lack of landmarks in the 2D views used to select areas of interest. CLEM has the potential to play

an important role here by facilitating the search for such areas of interest. In addition, CLEM is taking front stage in live cell imaging, where there is growing demand for fine structural information on processes whose dynamics have been recorded light microscopically.

1.1.2. Correlative Microscopy Today

The diversity of goals to be achieved by CLEM constrains the development of universally applicable protocols. For instance, correlating live cell imaging data of a fluorescent protein with an ultrastructural endpoint requires a different CLEM approach than if the main goal is to pinpoint a rarely occurring structure of interest for EM investigation. CLEM can also be used as an alternative for immuno-EM, or to locate structures for cryo-EM if high-resolution structural details are required. As a consequence of the diversity of applications, there are to date numerous methods to correlate LM and EM data, and more developments, improvements, and applications, are likely to follow. Depending on the purpose of the application, three groups of CLEM methodologies can be distinguished:

- Those that combine live cell imaging with ultrastructural information (see figure 1),
- Those that combine LM of fixed or immobilized samples with ultrastructural information (figure 2),
- Those that combine LM and EM data from the same sections (figure 3).

The following sections (1.1.2.1, 1.1.2.2. and 1.1.2.3, respectively) will discuss the possibilities, advantages, and disadvantages of each of these three groups. Special attention will be paid to the methodologies that were used throughout the studies presented in this thesis. Subsequently, three specific advances in TEM will be discussed in the context of CLEM, since these techniques are extensively used in combination with correlative experiments in this thesis:

- CLEM and electron tomography (section 1.1.2.4.),
- CLEM in an integrated setup (section 1.1.2.5.), and
- CLEM and cryo-electron microscopy (section 1.1.2.6.).

1.1.2.1. Correlating Live Cell Dynamics with EM Ultrastructure

The combination of CLEM and live cell imaging opens up the possibility to obtain ultrastructural information at a chosen moment during the progression of a dynamic process that was captured at LM resolution. Hence, instead of representing a static image with features of unknown pedigree, an EM image now becomes a high-resolution 'snapshot' in which the features have a known history. The interpretational gain is therefore immense. Nevertheless, as discussed in section 1.1, cells prepared for LM cannot be used for EM imaging and vice versa, and specialized protocols have thus been developed to correlate the same structures.

CLEM methods that combine live cell imaging and EM basically consist of five steps (figure 1): 1) incorporation of a fluorescent marker in cells, 2) LM imaging, 3) fixation/immobilization of the specimen, 4) preparation for EM, and 5) electron microscopy. The possibilities for combining live cell imaging and EM are mostly limited by steps one (fluorescence labeling) and five (electron microscopy). In step one, a fluorescent label is required that can be brought into living cells. Step five, on the other hand, is complicated because the precise correlation to the LM image needs to be made here. This can be a laborious task, since the two imaging modes provide very different views of the same structures. Below (1.1.2.1.1., respectively 1.1.2.1.2.), the current possibilities for these two limiting steps are listed and discussed.

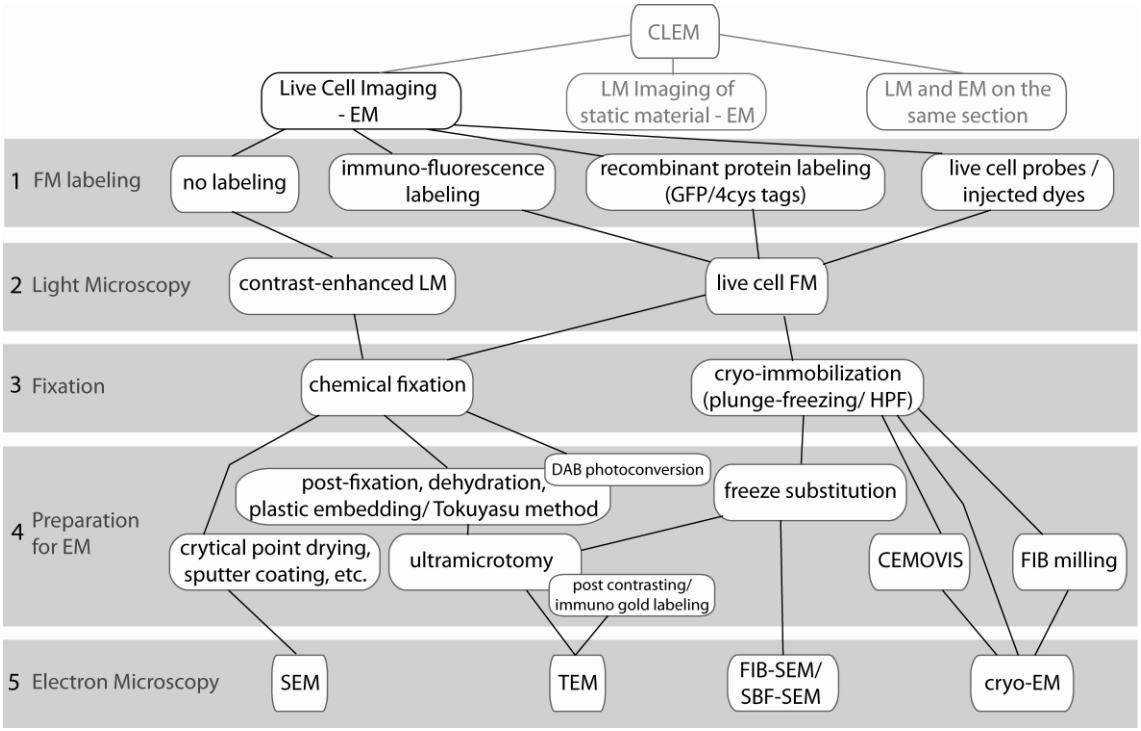

Figure 1. Schematic representations of CLEM workflows that combine live cell imaging with EM. For the sake of clarity, the flow chart has been divided into three parts on the basis of CLEM strategy. The present figure deals with strategies to combine live cell imaging with EM ultrastructure. Figure 2 focuses on CLEM procedures involving LM of static preparations, and figure 3 on LM and EM on identical sections.

1.1.2.1.1. Labeling methods for Live Cell Imaging

Biological specimens are notorious for their high intrinsic translucency for visible light. As a result, images produced by LM exhibit poor contrast. Specialized imaging techniques can be used to enhance contrast, such as phase-contrast imaging and differential interference contrast (DIC) (Salmon and Tran, 2003). These techniques can also be employed in CLEM experiments. For example, both McEwen et al. (1997), Mueller-Reichert et al. (2007), and Jones et al. (2008) have used DIC imaging to determine the mitotic state of cells, for subsequent TEM analysis on the mitotic spindle in the same cells.

Whereas these transmitted light LM techniques are suitable to visualize cells or cell compartments that intrinsically generate contrast, other cellular features can be localized using specific labels and fluorescence microscopy (FM). In this case, specific proteins, lipids, nucleic acids, ions, pH values, or membrane potentials are detected with a fluorophore.

Genetically encoded fluorescent indicators have become extremely popular amongst cell and molecular biologists as a tool to study the spatiotemporal expression of proteins in living cells. For this purpose, cells or whole organisms are genetically altered so that they express one or more proteins of interest ectopically with a built-in amino-acid sequence that serves as the fluorescent indicator.

Green Fluorescent Protein (GFP)

The most widely used sequence is 238 amino acids long and encodes for GFP (Chalfie et al., 1994) (see section 1.1.2.1. for details on GFP). An elegant example of live cell imaging of GFP in a CLEM study, is the work of Svitkina and Borisy on actin dynamics (Svitkina and Borisy, 1998; Svitkina et al., 2003). By combining live cell imaging of GFP-tagged actin with platinum replica EM, these authors were able to develop models explaining the molecular mechanisms by which lamellipodia and filopodia are formed. More recently, Spiegelhalter et al. (2010) combined live cell imaging of GFP with SEM as well as immuno-EM to elucidate the cellular localization and function of two proteins, myotubularin and amphiphysin 2, both of which are implicated in neuromuscular disorders.

Live imaging of GFP and CLEM can also be carried out on complete transgenic organisms. Using fluorescence microscopy, Sims and Hardin (2007) selected C. elegans embryo's rescued from a lethal mutation by the wildtype gene coupled to GFP. Following live imaging, the embryos were prepared for TEM by high pressure freezing (HPF), freeze substitution, Epon embedding, and sectioning.

Tetracysteine tags

Although GFP and its derivatives have been incorporated successfully in many different proteins without detectably interfering with the proteins' functions, the considerable size of the GFP

analogs (approximately 30 kDa) can pose a problem when coupled to smaller proteins (Evans and Martin, 2002; Frischknecht et al., 2006). An impact of tag size on protein function has for example been reported for yeast beta-tubulin (Andresen et al., 2004) and virion surface proteins (Das et al., 2009). Furthermore, Werner et al. (2009) performed a comprehensive screen of the localization of every open reading frame in C. crescentus. Of the 185 proteins that exhibited specific localization patterns with a GFP tag on the C-terminus, only 58 exhibited the same pattern when the tag was shifted to the N-terminus. For this reason alternative genetically encoded markers are sought that are smaller and thus less likely to interfere with the biological function of the tagged protein. A method that has become increasingly popular is protein tagging with a tetracysteine motif (see section 1.1.3.1. for a detailed description). This motif can bind to fluorescent bi-arsenical derivatives, the most widely employed being Flash (Fluorescein-based Arsenical Hairpin binder), and the red-light emitting ReAsH (Resorufin-based Arsenical Hairpin binder) (Machleidt et al., 2007; Tsien, 2005). The dyes are membrane-permeable and can therefore be used to label 4C tags in living cells (Gaietta et al., 2002; Hoffmann et al., 2010; Rudner et al., 2005). Comparable new labeling methods that are also receiving considerable attention are the proteins HaloTag (Los et al., 2008) and SNAP-tag (Keppler et al., 2003). These probes are likewise genetically conjugated to a protein of interest, and can bind to membrane-permeable fluorescent substrates. They provide a higher labeling specificity than the tetracysteine tags, but come at the price of a larger tag size. The latest progress on these and other live cell labeling tags was recently reviewed by (Hinner and Johnsson, 2010).

The 4C/bi-arsenical detection system can also be employed for live cell CLEM (Gaietta et al., 2011a). Sun et al. (2007) used FlAsH to follow cytochrome c bound to tetra-cysteine motifs, together with TMRE, a stain that monitors membrane potential, to characterize the progression of apoptosis in HeLa cells. Following electron microscopy of the same cells embedded in resin, it was possible to correlate the stage of apoptosis with mitochondrial ultrastructure.

Other fluorescent live cell probes

Besides genetic fluorescent tags, other labels that can be used for live cell CLEM, are 1) cell permeable dyes like mitotracker and lysotracker, 2) ion, pH or membrane potential indicators (Sun et al., 2007), 3) fluorescent probes for RNA detection (for a review, see Bao et al., 2009), 4) fluorochrome-conjugated proteins (Brown and Verkade, 2010), or 5) fluorochrome-conjugated antibodies directed against a protein of interest. In options 4 and 5, the fluorochromes can also be replaced by probes that are both fluorescent and electron dense, for example Alexa-gold conjugates, and quantum dots (QDs) (see section 1.1.3.2.). However, all the protein- or antibody conjugated probes are membrane impermeable, and can be used only for surface labeling of cells or for labeling of extracellular proteins. Alternatively, they can be employed for intracellular labeling via the endocytic pathway or via invasive techniques like micro-injection, lipofection or electroporation.

1.1.2.1.2. Making the Correlation in EM

As mentioned in section 1.1, several factors make it extremely laborious and time-consuming to retrieve in TEM mode the region of interest that was imaged in LM mode. First of all, several processing steps that separate the imaging modes can alter the appearance of the specimen, the most prominent of which are dehydration and sectioning. Dehydration can lead to shrinkage, thereby altering the position and shape of features in the specimen. Sectioning can also lead to distortions due to compression of the sample on the knife surface. Furthermore, a commonly encountered problem is that the optical sections recorded in LM do not match the ultrathin sections. The mismatch is due to differences in section thickness and -angle. Lastly, because the stains described for LM are mostly dye-based (chromophores and fluorophores), whereas EM stains employ electron-dense heavy atoms (osmium, uranium, and lead compounds), the same stain usually cannot be visualized both by LM and EM. In the worst-case scenario, it could result in a fluorescence signal being attributed erroneously to an ultrastructural feature that is not at all present in the optical section from which the fluorescence was recorded. Tools that aid in the retrieval of cells or cell structures after live cell imaging are therefore necessary.

Fluorescent/electron dense probes in live cells

For persuasive evidence that a structure in an EM section is the same structure as observed in the live cell, the fluorescence signal sometimes needs to accompany an electron-dense label. In this case, bifunctional probes can be used that are both fluorescent and electron dense (see section 1.1.3.2.). Due to the relatively large size of Alexa-gold particles and QDs in particular, it should be noted that they may alter the natural behavior of targeted proteins (Brown and Verkade, 2010; Howarth et al., 2008). Nevertheless, Alexa-gold conjugates enabled Brown and Verkade (2010) to study endocytic trafficking of transferrin and EGF by live cell CLEM.

A very recently described probe is the genetically encoded fusion protein ferritin-GFP, which can jointly be conjugated to a gene of interest (Wang et al., 2011). While the GFP functions in live imaging, the ferritin intracellularly binds iron that is supplemented to the culture medium, and can be visualized by cryo-EM. The probe is therefore the first bifunctional probe that can be visualized intracellularly in complete cells by both LM and EM without chemical fixation or membrane permeabilization.

As an alternative for the bifunctional probes, it is possible to incorporate an additional processing step to convert a fluorescent label into an electron-dense label. The currently available option for this is photooxidation of 3,3-diaminobenzidine (DAB). In this method, DAB forms an osmiophilic precipitate when it is oxidized by the free radicals that are formed in reaction to fluorescence (see section 1.1.3.3.). The photooxidation reaction can only be performed on chemically fixed material, and is therefore less suitable for cryo-CLEM and HPF.

Another option to enhance the correlation between an EM section and the prior live cell imaging data is to perform on-section immunolabeling using an antibody raised against the fluorescent protein. This technique will be discussed in section 1.1.2.3.3.

Support finder patterns

A method that has become common practice in CLEM, is to incorporate a finder pattern on the substrate where the cells are cultured on, and that is visible at both the LM and EM level.

For the combination of LM and SEM, gold can be evaporated through a TEM finder grid onto the surface of a glass coverslip (Sims et al., 2006; Svitkina and Borisy, 1998), or gold TEM finder grids can be glued to glass cover slips on which the cells grow (this thesis, chapter two).

Because LM and SEM can be done on the same, whole mount specimens, and both permit the overview of quite large specimens, it is relatively easy to find back the exact cells compared to correlations using TEM. In the case of TEM, a step of ultrathin sectioning must be incorporated between LM and TEM imaging, which further complicates the correlation. Again, a gridded glass cover slip can simplify the search. When the grid pattern is engraved in the glass, the resin that embeds the cells for EM will mirror the grid pattern on the resulting block face (Kreplak et al., 2008; van Rijnsoever et al., 2008). In this way, the position of the cells imaged in LM can be retrieved, and serial sections can be cut in these areas.

Whereas cells grown on gridded glass coverslips need to be chemically fixed for EM preparation, other cell carriers can be used if live cell imaging is followed by vitrification techniques such as plunge freezing and HPF (see section 1.1.2.3.1.). For instance, gold finder grids can be used as a cell support if live cell imaging will be followed by plunge freezing. For HPF, special carriers have been adapted to contain a grid pattern as a localization tool for the LM and TEM steps (Brown et al., 2009; Guizetti et al., 2010; Jimenez et al., 2010; Spiegelhalter et al., 2010). Although these tools aid in the correlation, the combination of live cell imaging and vitrification is complicated by the need to transfer the live samples from the fluorescence microscope to the vitrification device. This transfer step results in a time lag between fluorescence imaging and vitrification that ranges from half a minute to several minutes. Applications suitable for this approach are therefore restricted to, for instance, the localization of transfected cells or labeled organelles, or relatively slow cellular processes like mitosis or cell migration. One has to keep in mind that the cells are also subjected to changes in temperature, pH and air composition during the transfer step, which can give rise to further changes in cell dynamics and behavior. To reduce the time lag, a ‘rapid transfer system’ has been developed and employed for live cell imaging in combination with HPF (McDonald, 2009). In addition, an integrated fluorescence microscope and plunge-freezing device has been developed that eliminates the transfer step completely (R.I. Koning, personal communication). The instrument, which is currently being tested, contains a fluorescence microscope incorporated into the climate chamber of a plunge freezer. Samples are therefore imaged in a stably controlled environment and are vitrified within ~5 seconds.

When small invertebrate organisms are used for CLEM experiments, retrieving a region of interest poses new challenges due to the increased size and complexity of the samples. Although Muller-Reichert et al. (2008) managed to follow the mitotic states of C. elegans embryo's using GFP-tubulin, regions of interest could only be retrieved in TEM after careful serial sectioning through the complete adult worm carrying the embryos. Sims and Hardin (2007) similarly performed serial sectioning of isolated C. elegans embryo's, which they immobilized in agarose. The serial TEM sections could then be matched with the FM images obtained in the live embryos. A difficulty, in this case, is the difference in orientation of a live embryo compared to the embryo as it is sectioned for TEM. Very recent CLEM techniques that face the same orientation problems are focused ion beam (FIB) milling, or alternatively serial block face (SBF) sectioning, combined with SEM (FIB-SEM, respectively SBF-SEM) (De Winter et al., 2009; Denk and Horstmann, 2004; Heymann et al., 2006). In these techniques, a slice of a resin block is removed and the revealed surface is imaged in the SEM using back-scattered SEM imaging. Cutting and imaging are sequentially repeated to automatically collect a set of images through a volume of the sample, which can be reconstructed into a 3D volume. The advantage of the large volume imaging does come at the expense of EM resolution; up to 4 nm in the lateral, and maximum 10 nm in the axial directions. Using these methods, Armer et al. (2009) correlated fluorescence imaging of angiogenesis and anastomosis in live zebrafish embryos with SEM ultrastructural information from the exact sites of endothelial cell contact. The method therefore elegantly enabled correlative imaging of a large volume of the samples. However, defining the directionality of the sample in the resin block, and overlaying the FM and EM data were again cumbersome. The directionality was determined by first cutting TEM sections from the block face to reveal anatomical landmarks in the embryos. These landmarks served to orient the sample correctly in the FIB-SEM or SBF-SEM. As a possible tool for improvement, Kolotuev et al. (2009) created a flat embedding protocol for small invertebrates. The authors used a laser dissection microscope to carve a grid around C. elegans embryos embedded in epoxy resin. The grid was used to determine the angle in which the resin should be sectioned, so that the sectioning direction was parallel to the optical sections acquired before by FM. The known directionality of the TEM sections facilitated the correlation with live images.

1.1.2.2. Correlating LM of Fixed Material with EM Ultrastructure

A common method of CLEM employs fluorescence imaging of chemically fixed samples, followed by preparation for EM. The immobilized material permits a more detailed analysis of rapid dynamic processes, a 'snapshot in time'. It can therefore also be desirable to complement studies on live material with observations on static preparations. In addition, whereas live cell imaging can be performed on only one or several locations in a sample, fixed material allows the prolonged examination of complete samples. Its information can therefore be used to the fullest. Common applications are to locate a rare event in large samples (Capani et al., 2001; Hekking et al., 2009), to couple a fluorescence signal to ultrastructural morphology (chapter three of this thesis), or to discern transfected cells from non-transfected cells. A recent example of the latter application is given by (Volkova et al., 2010), who studied the influence of the expression level of GFP-tagged nuclear envelope proteins on the natural morphology of the cell. In fixed monolayers of Hela cells, the authors could conclude that the expression level, observed by FM, determined the severity of disruption of the morphology of the nuclear envelope.

Chemical fixation also opens up opportunities for CLEM of large tissue samples like biopsies. Fixed tissue biopsies can be labeled for exposed epitopes (see for example Jiao et al., 2010) as well as intracellular epitopes by cell permeable dyes and histochemical stains (Vogels et al., 2009), or after invasive techniques such as detergent treatment, micro-injection, lipofection, and electroporation. Examples of such applications can be found in Hohensee et al. (2008) and Capani et al. (2001), who studied nervous tissue of moth and rat, respectively. In the latter, actin was visualized by injection of fluorescent phalloidin into specific neurons, which elegantly revealed their long, extending axons and dendrites.

The fluorophores used for imaging static preparations are largely identical to the probes used in live cell imaging, since most preserve their fluorescence after the fixation step, e.g. GFP and Alexa dyes. However, fixation also provides an extra opportunity for LM labeling of cells or tissues (figure 2), the possibilities of which are discussed below. To retrieve the fluorescence signals in EM, the same complications arise as after live cell imaging. These complications, as well as methods to enhance the correlation procedure, are described in section 1.1.2.1.2.

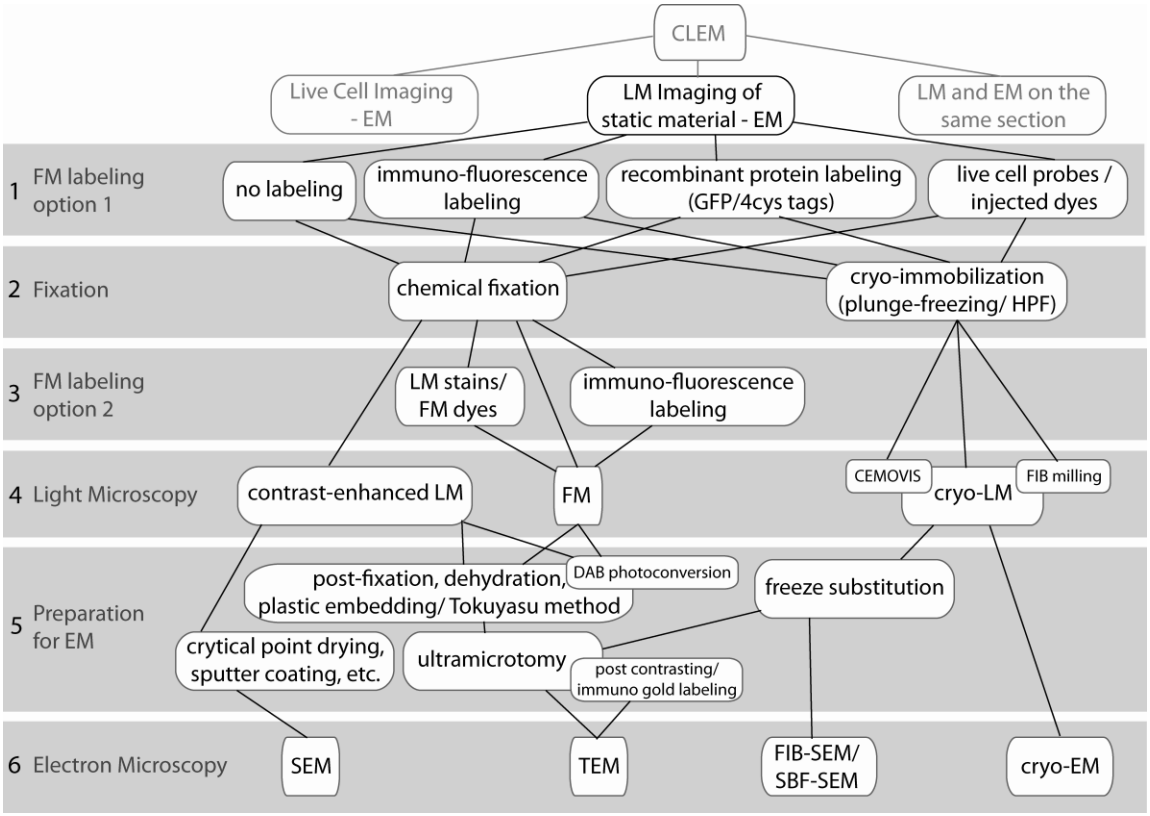

Figure 2. Schematic representations of CLEM workflows that combine imaging of static LM preparations with EM. Since light microscopy is performed after fixation, there are two optional steps where FM labeling can take place: before and after fixation.

The Golgi-impregnation method

One of the first CLEM methods described for fixed tissue blocks is the Golgi-impregnation method, which is used to stain neurons (Fairen, 2005; Peters, 2002). Up to this date the Golgi stain remains one of the few stains that are visible by LM as well as EM. Due to their considerable size, neurons are readily classified at the LM level, while EM resolution is required to characterize their synaptic connectivity (Valentijn et al., 1989). The Golgi-method randomly impregnates in tissue blocks a subset of neurons and glial cells with a metallic deposit. At the LM level, impregnated cells appear dark and cell bodies with their processes (dendrites and axons) can be viewed in three dimensions. The metallic impregnation is electron dense, so that the same neurons can be identified at the EM level. Several enhancements to the technique, such as de-impregnation and gold toning, result in finer ultrastructural detail (Fairen, 2005).

Today the Golgi-EM technique has fallen from grace, as alternative, more predictable methods are available. These include intracellular or juxtacellular injection of fluorescent tracers (e.g. lucifer yellow), and loading of synaptic vesicles with FM 1-43 or one of its spectral variants (Cochilla et al., 1999; Stewart, 1981). Photooxidation of DAB can then be used to obtain an electron-dense label for EM analysis (Capani et al., 2001; Maranto, 1982; Nikonenko et al., 2005). Another approach is to perform pre-embedding labeling of a fluorescent tracer together with silver-enhanced ultrasmall gold (Morozov et al., 2002).

Immunocytochemistry using fixed samples

Chemical fixation also allows the detection of intracellular epitopes by immunocytochemistry. Immunocytochemistry is often seen as a meaningful addition to the study of genetically tagged proteins. Since these proteins are always overexpressed in cells or tissues, they may affect in unpredictable ways their own behavior and that of their endogenous counterpart (Andresen et al., 2004; Hanson and Ziegler, 2004; Volkova et al., 2010). Therefore, there is a constant necessity to obtain feedback from non-transformed cells or tissues.

The most widespread detection system is based on the recognition of unique epitopes in proteins by monospecific antibodies. The antibodies can be visualized by fluorochromes, gold particles, a fluorescent/electron dense probe (Alexa-gold conjugates, QDs or fluoronanogold, see section 1.1.3.2.), or the product of an enzymatic reaction (e.g. horse radish peroxidase (HRP)/DAB, also see section 1.1.3.3.) (Sternberger and Sternberger, 1986). Often, the label is not conjugated to the primary antibody but to a secondary detection molecule that recognizes the primary antibody; the secondary molecule can be an antibody as well, or the bacterially derived protein A and protein G.

A drawback of this procedure is that it usually requires membrane permeabilization, to ensure accessibility of intracellular epitopes to the detection molecules. In addition, only mild chemical fixatives can be used as the stronger fixatives suppress the immunogenicity of the specimen. Weak fixation and permeabilization have a negative impact on the ultrastructural preservation. It follows that protocols for immuno-EM necessitate a careful balance of antigenicity and preservation.

Alternatives to immunodetection

In addition to antibody-based detection systems, there are a number of compounds that display high affinity for specific proteins and that can be conjugated to fluorescent or other types of indicators. Classic examples are the cytoskeletal markers, phalloidin and paclitaxel. Phalloidin is a toxin derived from the death cap mushroom, Amanita phalloides, and binds specifically to filamentous actin (Small et al., 1999; Vetter, 1998; Wulf et al., 1979). It has been used for instance, conjugated to an alexa dye, in CLEM by Jahn et al. (2009) to image actin organization in breast cancer cells, and conjugated to eosin to study actin in dendritic spines embedded in brain tissue (Capani et al., 2001). Because phalloidin and eosin are both small molecules, the latter study shows that they can penetrate chemically fixed cells and tissues without the need for membrane detergents. Paclitaxel, better known by its trade name Taxol, is a compound derived from the bark of the Pacific yew tree, Taxus brevifolia, and labels microtubules (Manfredi et al., 1982).

1.1.2.3. CLEM on ultrathin sections

Unless a specimen is thin enough to be visualized directly by TEM, a step of ultrathin sectioning must be incorporated between LM imaging and EM imaging. As discussed in section 1.1.2.1.2., this step can render a correlation problematic. Ideally, part of the LM signal will remain retrievable from the thin EM sections, so that correlations can be made more directly. Several options are available to perform LM detection on ultrathin sections; these include labeling of live or fixed cells with a tag that remains fluorescent after processing for EM and in ultrathin sections (section 1.3.3.2.), and post-embedding (immuno)labeling of the ultrathin sections with new LM labels (sections 1.3.3.3. and 1.3.3.4.). The different strategies are recapitulated in figure 3. The sectioning step exposes the cell interior to the section surface, which offers an additional possibility to label intracellular proteins without the need for membrane permeabilization. A spin-off of the on-section fluorescence studies was the realization that due to their thinness (typically 50-80 nm), ultrathin sections yield very sharp fluorescence images that lack z-axis blur (Mori et al., 2006). For comparison, the optical section thickness of a confocal laser scanning image is typically around 500 nm.

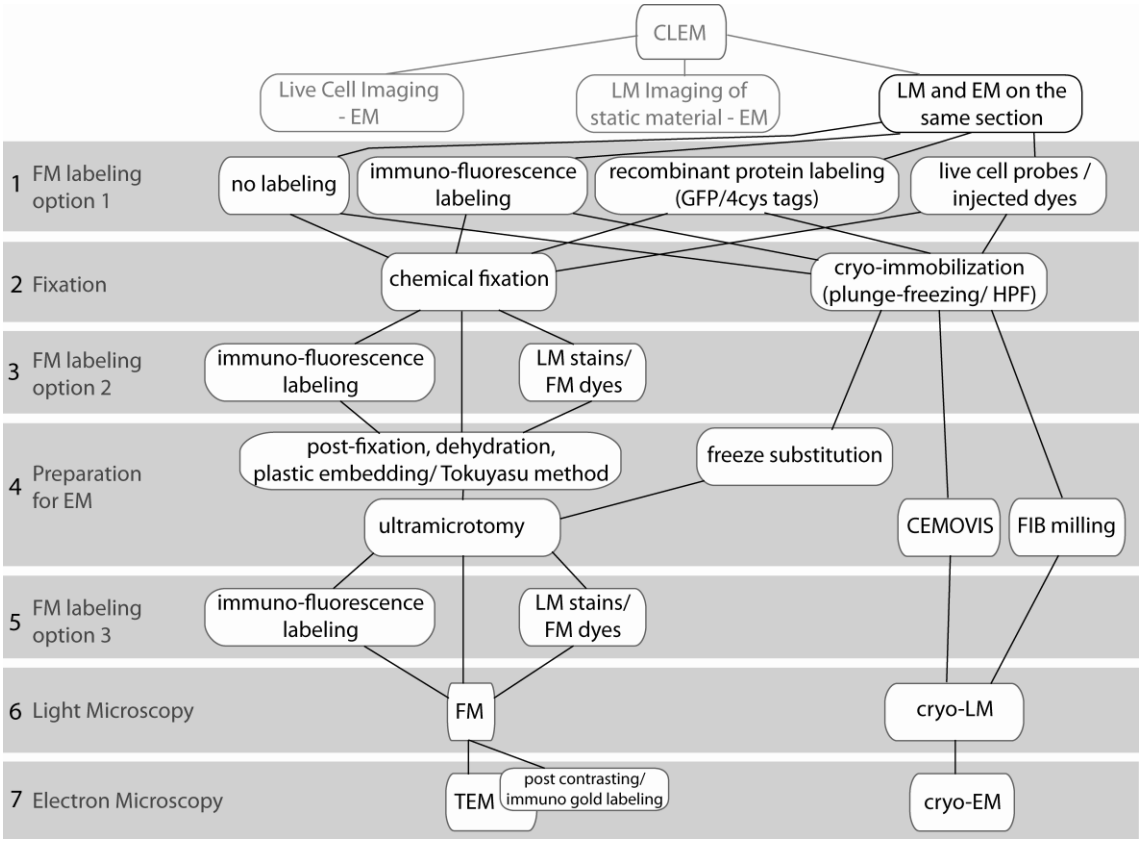

Figure 3. Schematic representations of CLEM workflows where both LM and EM are performed on the same sections. There are three optional steps where FM labeling can take place: before and after fixation, and FM labeling on the EM sections.

Since the same sections are used in both imaging modes in this CLEM method, retrieval of correlated structures at the TEM level is much simplified. The grid bar patterns and the section edges, both of which can be observed in LM, can for instance serve as reference points to locate the position of labeled structures in TEM. In the case of more difficult correlations, such as structures with unknown ultrastructural morphology or tiny structures like single protein complexes, more exact retrieval methods may be required. For this, software routines are available that translate coordinates between the imaging modes (one software program is described in chapter 4 of this thesis). These software routines have a positioning accuracy of at best ~500 nm. Alternatively, it is possible to combine a fluorescence signal with an electron dense label.

Cryo-immobilization and freeze-substitution is the preferred method for specimen preparation for TEM, as it results in improved morphological preservation and immunoreactivity (Shiurba, 2001). This preparation method will be discussed first, before going on to the different CLEM methods.

1.1.2.3.1. Cryo-immobilization and Freeze Substitution

Cryo-immobilization is achieved via vitrification, a process whereby the specimen is cooled very rapidly to liquid nitrogen temperatures, so that the water in and around the specimen becomes vitreous, i.e. an amorphous or non-crystalline liquid (Costello, 2006; Dubochet et al., 1988). In the process, all molecules become immobilized without any alteration in their location or chemical composition. This is sometimes referred to as cryo-fixation, which is a confusing term because it wrongly suggests that the molecules are cross-linked.

The most commonly used vitrification methods are plunge-freezing and HPF (Braet et al., 2007; McDonald and Auer, 2006; McIntosh et al., 2005). The former consists of the plunging of the specimen into a cryogen, ethane or propane, which is cooled by liquid nitrogen; and the latter uses high pressure (around 2100 bar) combined with rapid freezing to prevent ice crystal formation. Plunge freezing is limited by a vitrification depth of ~15 µm, and is therefore suitable only for thin cells and suspensions of macromolecules. HPF, on the other hand, permits cryo-immobilization of samples up to 0.2 mm thick, and is therefore also suitable for tissue fragments such as biopsies.

Whereas chemical fixation is usually followed directly by LM imaging, this is seldom the case after vitrification. This is obviously caused by the necessity to keep the sample under the devitrification temperature of around -135°C. Instead, vitrification is most often followed by freeze substitution (FS), and embedding in plastic. The principle behind freeze-substitution is to replace the ice in a vitrified specimen by an organic solvent (e.g., acetone or methanol) while a low temperature is maintained (-80 to -90 °C) (Giddings, 2003; Shiurba, 2001). As the temperature is slowly raised, fixatives added to the solvent will start to cross-link biomolecules in the sample. Subsequently, the

sample is infiltrated with resin, and the resin is polymerized either by UV-illumination at low temperatures (-30 °C) or by warming (60 °C).

1.1.2.3.2. Preservation of LM probes in embedded tissue

Freeze substitution was long thought to proceed at the expense of fluorescent labels or dyes. However, several adaptations of FS protocols have been published that retain fluorescence in the resin-embedded block, or even in thin or ultrathin sections. Hyde et al. (2003) reported that several non-fixable dyes do retain their fluorescence during aldehyde-free freeze-substitution and embedding in Spurr's resin. Around the same time, Luby-Phelps et al. (2003) were the first to describe that GFP fluorescence survives chemical fixation and embedding in LR White. Adjacent 1 µm thick and ultrathin sections were cut from preparations of zebrafish eyes and viewed using LM, respectively TEM after immunolabeling. This adjacent section approach was later also used by Keene et al. (2008) in their study of GFP/YFP fusion proteins. A setback of the approach is obviously that structures identified in the LM sections, can be absent in the following thin section. Later, several adapted freeze substitution protocols were shown to preserve fluorescence signals even in thin and ultrathin resin-embedded sections (Kukulski et al., 2011; Nixon et al., 2009; Sims and Hardin, 2007).

In addition to these methods, another established method of CLEM in freeze substituted material involves the inclusion of low molecular-weight fluorescent dyes, such as acridine orange and saffranin O, in the substitution medium (Biel et al., 2003; Pfeiffer et al., 2003; Wilke et al., 2008). The rationale for this method is that since molecules with a molecular weight up to 700 Da are washed out of the sample during freeze-substitution (Pfeiffer et al., 2000), similarly small molecules can also infiltrate the sample. The stains provide visual clues of gross features that can be used as landmarks in a multimodal coordinate system. They are especially suitable for orientation in complex tissues. As with other fluorescent probes, the dyes are only preserved when osmium tetroxide postfixation is omitted, while small amounts of uranyl acetate are tolerated. Usually, the fluorescence signals are recorded by confocal laser-scanning microscopy through the block face of a specimen block. Ultrathin sections are subsequently cut from the same block face and EM images are then correlated with the corresponding slices in three-dimensional reconstructions of confocal image stacks (Biel et al., 2003; Wilke et al., 2008). The protocol was therefore rather cumbersome and laborious. Chapter two of this thesis shows that certain stains present in the block-face are still visible in ultrathin sections, thus allowing for the correlation of LM and EM in the exact same slice. Although in the same chapter we do not succeed to label the thin sections for immuno-fluorescence microscopy, Wilke et al. (2008) shows that this is under certain conditions possible.

1.1.2.3.3. Immuno-labeling EM sections to detect previously observed fluorophores

For TEM, immunogold labeling on ultrathin sections is the most widely used method to detect epitopes on ultrathin sections. The labeling is most commonly performed on frozen-thawed sections, according to the technique by Tokuyasu, since this method best preserves antigenicity. The Tokuyasu method utilizes ultrathin sections of chemically fixed material, cut by means of cryo-ultramicrotomy; the labeling and microscopy, however, are performed at room temperature (Liou et al., 1996; Peters and Pierson, 2008; Slot and Geuze, 2007; Tokuyasu, 1973). The method enabled Zeuschner et al. (2006) to analyze COPII-coated transport carriers between the endoplasmic reticulum and the Golgi apparatus. Immunogold labeling can also be performed on ultrathin sections of resin-embedded specimens. Acrylate- and methacrylate-based resins can be directly labeled, while epoxy-resins require additional treatment, such as surface etching with sodium ethoxide, for antigen retrieval (Groos et al., 2001; Newman and Hobot, 1999). However, etching is an invasive technique that goes at the expense of ultrastructure, whereas it does not always result in successful labeling.

Immunogold labeling can also be employed in CLEM experiments to detect the fluorescent probes that yielded the LM signal but whose fluorescence became quenched during processing for TEM. The feasibility of this approach was first demonstrated in the early 1990s by van Dam et al. (1991), who used gold-conjugated antibodies against fluorescein isothiocyanate (FITC) to detect at the ultrastructural level a protein (gut-associated circulating cathodic antigen) in the worm, Schistosoma mansoni. More recently, Coleman et al. (2006) reported that the fluorochrome Alexa Fluor 488 remains immunoreactive even after fixation with glutaraldehyde and osmium tetroxide, embedding in epoxy resin, and etching with sodium ethoxide. They demonstrated that it was thus possible to perform pre-embedding immunolocalizations of a transporter and an ion channel in rat kidney, and to detect the Alexa Fluor 488 label subsequently in semithin and thin plastic sections with anti-Alexa Fluor 488 antibodies. These antibodies were in turn detected by secondary antibodies conjugated either to a fluorophore for LM or colloidal gold for EM. We have not been able to reproduce these data in our laboratory (Agronskaia and Valentijn, personal communication). Oberti et al. (2010) performed a comparable study, injecting dextran-coupled Lucifer yellow, Alexa Fluor 647, and rhodamine into different brain areas, to study their neuronal interconnections. After tissue embedding in Durcupan, thin sectioning, and treatment with periodic acid to oxidize the durcupan, the fluorophores could again be detected with fluorescent antibodies on thin sections.

Ultrathin Tokuyasu sections also allow for immuno-labeling of fluorescent proteins like GFP (Koster and Klumperman, 2003; Polishchuk et al., 2006; Verdijk et al., 2005; Westbroek et al., 2003). Usually, the preparation of cells for cryosectioning involves enzymatic or mechanic dispersion and centrifugation to obtain a cell pellet that is suitable for freezing. However, these steps will obliterate the spatial coordinates needed for correlating cells at the LM and EM level. To

circumvent such problems, Oorschot et al. (2002) have developed a flat-embedding method that allows for ultracryotomy of cultured cells while preserving their topology. The group used the flat embedding protocol to combine live cell imaging of the lysosomal marker LAMP-1-mGFP, with immuno-gold labeling against the mGFP on Tokuyasu cryo-sections from the same imaged cells (van Rijnsoever et al., 2008). Spiegelharter et al. (2010) elegantly demonstrated that the protocol can be adapted for HPF and freeze substitution/lowicryl HM20 embedding.

1.1.2.3.4. On-section LM labeling

On-section LM stains

Numerous histological stains can be applied to resin-embedded tissue sections, and are even compatible with EM stains. They provide visual clues at the LM level to reveal histo-architectural features, which can aid in general orientation and identification of specific areas (McNary et al., 1964). However, the thinness of ultrathin sections required for EM reduces the uptake of LM stains thereby diminishing the intensity. Ultrathin sections must in this case be alternated with semithin sections for LM staining. Jones et al. (1982) reported that toluidine blue is a suitable stain for epoxy sections of osmicated tissue if the section thickness is above 100 nm. The toluidine blue stain is useful in surgical histopathology, as it allows for the LM detection of areas of diagnostic importance in thin sections of human biopsies. Chapter two of this thesis describes an on-section fluorescent stain suitable for ultrathin sections. In order to preserve the fluorescence, heavy metal EM stains have to be reduced to a minimum.

Correlative Immuno-Detection Methods

For biological questions that call for the localization of specific proteins, the post-embedding immuno-gold labeling techniques can be adapted to allow on-section CLEM. This method is most efficient on Tokuyasu cryo-sections, or surface etched Lowicryl sections, as described in section 1.1.2.3.3.

The most commonly employed methods use an immune-probe that can be visualized by LM, for instance fluorescent antibodies, or antibodies conjugated to fluorescent-electron dense probes (Groos et al., 2001; Schwartz and Humbel, 2007). Robinson and Takizawa, for example, applied immuno-labeling with fluoronanogold (section 1.1.3.2.) directly on cryo-sections in their study of the human placenta (Robinson and Takizawa, 2009; Takizawa and Robinson, 2006). Another example comes from Vicidomini et al. (2008), who used ultrathin cryo-sections to examine Russell-body like structures induced in HeLa cells by transfection with mutant immunoglobulin. Following primary antibody labeling for the immunoglobulins, the authors applied a combination of fluorescent secondary antibodies and protein A-gold as a step for combined FM and TEM labeling. As alternative to the gold particles, QD- or HRP-conjugated antibodies can also be used.

1.1.2.4. CLEM and Electron Tomography

Electron tomography is a technique that generates a 3D reconstruction, i.e., a tomogram, from a series of 2D images taken of a 3D object at different viewing angles (Koster et al., 1997; McEwen and Marko, 2001). As its name indicates, electron tomography deals with 2D images that are acquired with an electron microscope. The high resolution of TEM enables electron tomography to model structures that are as small as macromolecules. The different 2D viewing angles are obtained by tilting the specimen in the electron beam while acquiring images at discrete tilt angles (McIntosh et al., 2005). With increasing tilt angles, the path length of the electron beam through the specimen increases gradually, up to a point where the majority of the electrons are scattered and image detail is lost. In practice this means that the maximum usable range of tilt angles goes from -70 to 70 degrees. As a consequence, tomograms display a so-called 'missing wedge' artifact, due to the lack of 3D information at higher tilt angles. The missing wedge causes a distortion in the high tilt range of the objects in the tomogram, which results in the visual disappearance of their ultrastructural. Fortunately, the missing wedge artifact can be greatly reduced by tilting the specimen around two orthogonal axes, resulting in a dual-axis tomogram (Marsh, 2005; McIntosh et al., 2005).

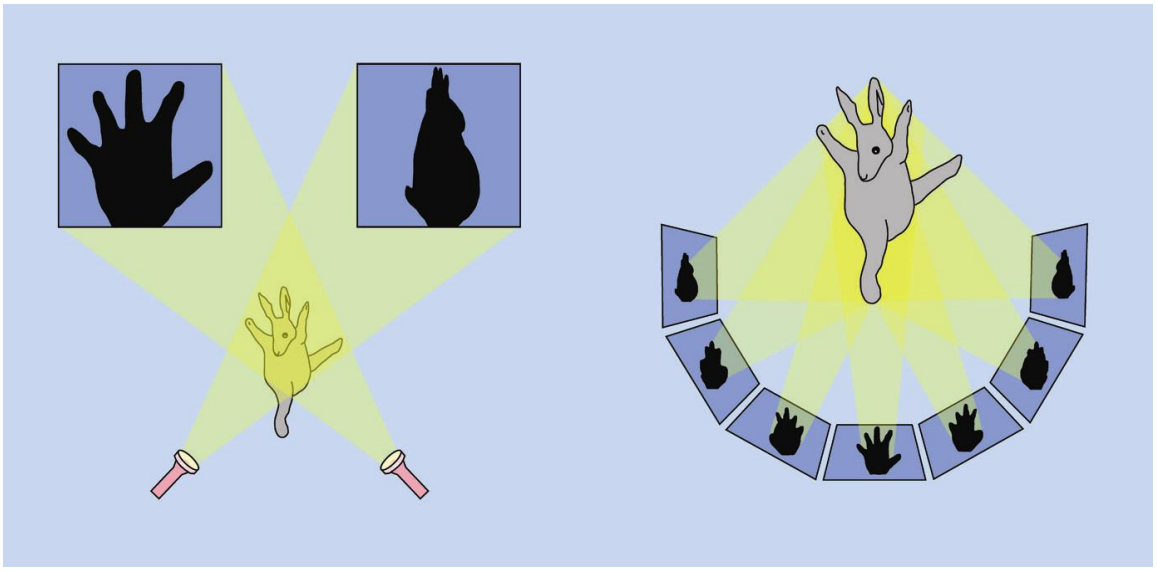

Figure 4. The principle of electron tomography. Depending on the projection angle of the light source, the 3D rabbit will cast a different 2D shadow. By analogy, a 3D biological sample will generate varying 2D projections when it is tilted in the electron microscope. By back-projection of a series of 2D images into a virtual 3D space, the source 3D object can be reconstructed. (Loosely based on a cartoon by John O'Brien, which appeared in The New Yorker Magazine).

The development and implementation of electron-tomography techniques goes hand in hand with the ongoing progress in computer-assisted microscope automation, digital image acquisition, and computing resources (Leapman, 2004). A powerful computing environment is important not only to display the large data sets tomograms consist of, but also to calculate the 3D reconstructions from the 2D data. Several algorithms are available to generate tomograms, but the most commonly used are based on the principle of back-projection (figure 4).

With an appropriate viewer program, tomograms can be browsed slice per slice, and along any of the three axes. Each tomographic slice represents an image that is just a few nanometers thick. The resolution is comparably high on all three axes. Conversely, in a conventional 2D TEM image the lateral resolution is also in the order of a few nanometers, but the z-axial resolution is limited by the section thickness (typically 50-70 nm; figure 5) (McIntosh et al., 2005). The fine structural detail in three dimensions revealed by a tomogram can be overwhelmingly complex. It is therefore common practice to generate graphic models in which features of interest are accentuated by different colors; shadows and color gradients are applied to simulate lighting and perspective (for some colorful examples, see refs. Knoops et al., 2008; Marsh, 2005; Trucco et al., 2004). These graphic representations can be drawn by hand or generated with the assistance of image processing routines such as an edge detection filter.

Electron tomography is still too time-consuming to allow for 3D browsing of a specimen. For this reason, areas of interest need to be selected in 2D views. If the electron accelerating voltage of the electron microscope is sufficiently elevated or if an energy-filter is used, high-resolution electron tomograms can be made from specimens up to 400 nm thick, and yet thicker specimens have been imaged with special high-voltage electron microscopes (Glauert, 1974; Kamioka et al., 2009; Ladinsky et al., 1994). Even at more standard specimen sizes (around 200 nm thick) for electron tomography, it can be difficult to find areas of interest in a 2D image, due to the stacking of electron-dense features that obscure the image. In this respect, CLEM has the potential to facilitate the search for areas of interest, as the section thickness will not obscure photon-based imaging. Crucial for this application is the availability of fluorescence labeling protocols that are compatible with thin plastic sections and TEM processing, or alternatively, an electron dense label that associates an earlier observed fluorescence signal.

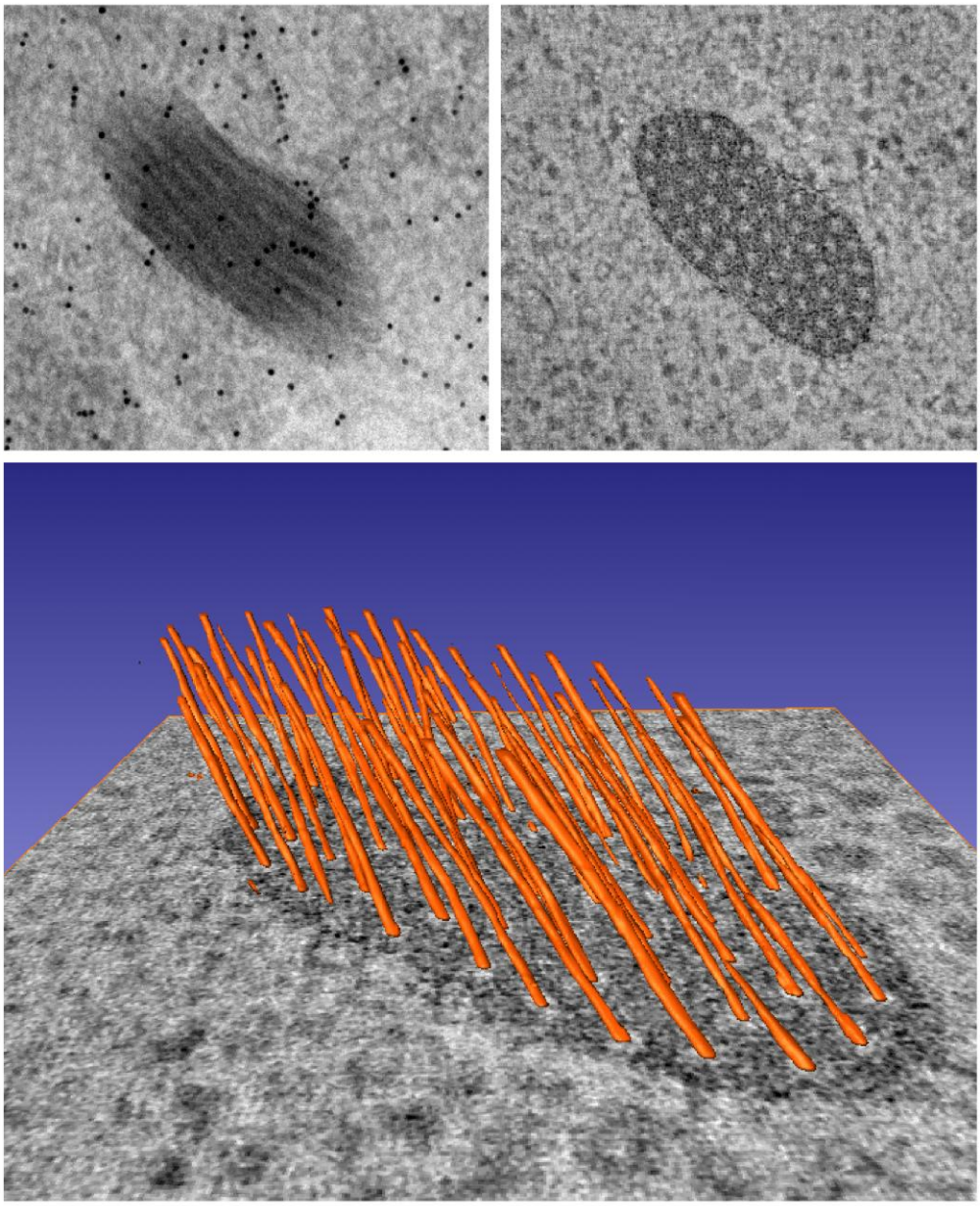

Figure 5. The power of electron tomograpy. Images illustrate alternative views of a Weibel-Palade body, a specialized secretory granule, in a human umbilical vein endothelial cell. The Weibel-Palade body measures approximately 450 by 200 nm. The top left image represents a standard 2D TEM image. Note the ill-defined boundaries of the Weibel-Palade body, which appears to contain 7 longitudinal striations running in parallel. The black dots correspond to 10-nm gold particles; they were applied on the section as fiducial markers to aid in the alignment of the tomographic images. The top right image represents a tomographic slice of 4 nm thick taken from the reconstruction of the Weibel-Palade body after imaging by dual-axis tomography. Note that the boundaries are much sharper, and that the organelle now contains 58 cross-sectioned tubules. The bottom panel shows a 3D model of the internal organization of the Weibel-Palade body, superimposed on a tomographic slice. Evidently, the tomography data reveal important features that are masked in the 2D image.

1.1.2.5. CLEM in an integrated setup

Some of the technical challenges encountered with CLEM, as described in this Introduction, could be overcome if LM and TEM were performed in an integrated microscopy setup using thin sections. The main advantages of using an integrated setup over two separate setups are i) that the coordinates of both imaging modes are linked, thus saving time in the localization of previously identified regions of interest, and ii) that manual handling steps are avoided, which can potentially damage the fragile TEM grids or sections.

To date, two fully integrated devices have been described. The now defunct LEM 2000, a combined light and electron microscope (Akashi Seisakusho Ltd., Tokyo, Japan), was equipped with a microprocessor that enabled the recording of coordinates for multiple areas of interest selected in LM mode. The coordinates could then be retrieved in TEM mode to permit precise correlation with the LM fields of view. The LEM 2000 used a larger grid size (7 mm in diameter; for comparison, standard grid size is 3 mm), allowing for the observation of larger sample areas (Nelson, 1986). These features made the LEM 2000 an instrument of choice for diagnostic CLEM (Jones et al., 1982). At present, it would be the right time to resurrect a combined light and electron microscope system, taking advantage of modern digital imaging techniques, microscope automation, and ever increasing computing resources. The LM mode of the LEM 2000 allowed only widefield images to be taken. Therefore it was necessary to generate contrast by staining the ultrathin sections with toluidine blue. A modern version of an integrated CLEM system should also include the possibility to visualize fluorescence signals in order to increase the palette of stains and probes that can be applied to specimens. As a matter of fact, such an integrated system has recently been developed. Named ILEM, for Integrated Light and Electron Microscope, it comprises a laser scanning fluorescence microscope (LSFM) built into a commercially available TEM (Agronskaia et al., 2008). The principle of the ILEM is illustrated schematically in figure 6. The laser scanning fluorescence microscope of the ILEM is a retractable unit mounted on one of the TEM's side ports. Imaging in LM and TEM mode is done sequentially, using the original sample stage and specimen holder of the TEM. Inter-modal coordinate retrieval is fully automated via software implementation. The lateral optical resolution of the LSFM is estimated at 0.55 µm for an excitation wavelength of 470 nm. The power of the ILEM system has been demonstrated already using several different biological samples (Agronskaia et al., 2008; Karreman et al., 2009), including the samples described for CLEM in chapter two of this thesis. In chapter five, the ILEM is shown to be suitable for cryo-CLEM approaches as well, simply by replacing the standard room-temperature holder by a cryo-EM holder. This integrated approach obliterates the disadvantages that accompany other cryo-CLEM procedures, such as ice contamination on the sample and risky specimen transfers.

The ILEM will be useful in many areas of biomedical research, including the diagnostic CLEM that the LEM2000 was developed for. With the introduction of the LEM 2000, it was reported that

CLEM can complement diagnostic EM techniques as a means to facilitate the search in biopsies for areas of disease that require ultrastructural analysis. Thus at the LM level tissue samples can be surveyed to obtain rapidly relevant information on the orientation, architecture, and location of tissue components (Jones et al., 1982). It is then a matter of selecting areas of interest, which can be zoomed into at the EM level.

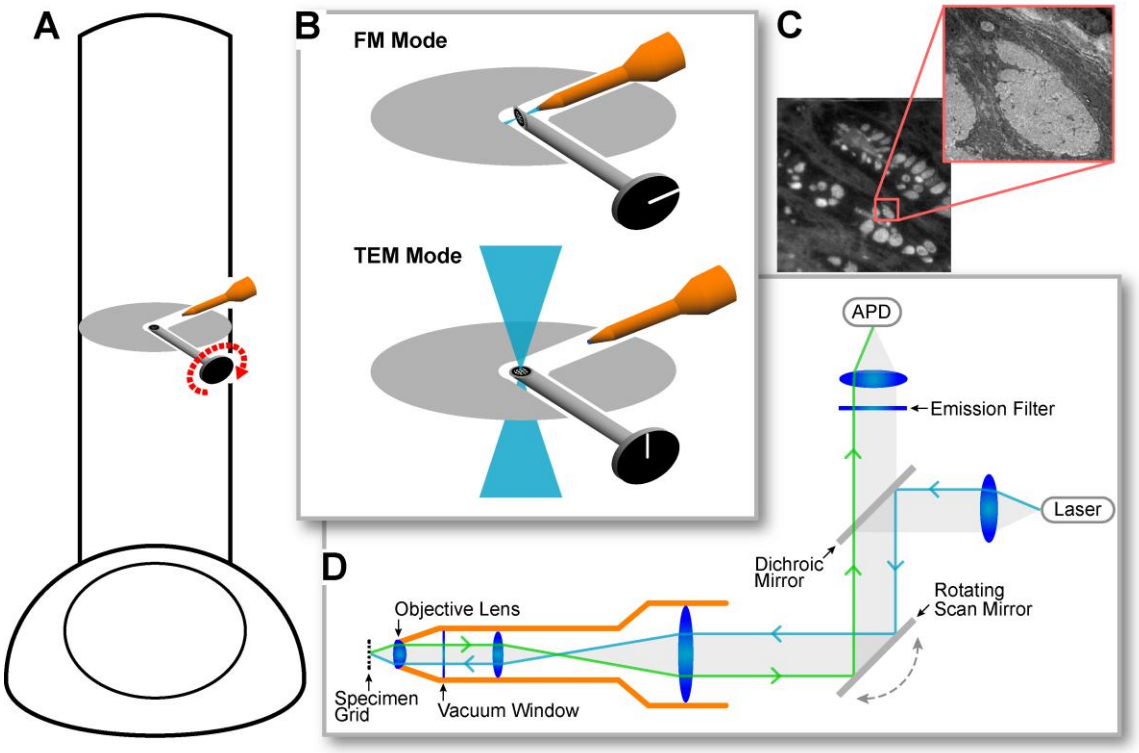

Figure 6. Schematic representation of the Integrated Light and Electron Microscope (ILEM), which was recently developed as a novel approach to CLEM. The ILEM comprises a laser-scanning fluorescence microscope (LSFM) that is mounted as a retractable unit (depicted in orange) on one of the side ports of a commercial TEM (panel A). The LSFM is positioned perpendicular to the TEM specimen holder. In fluorescence microscopy mode (FM mode), the specimen and specimen holder are rotated 90° so that the specimen can be scanned by the laser beam of the LSFM unit (Panel B). In TEM mode, the LSFM unit is retracted and the specimen tilted to the 0° position, allowing for imaging with the electron beam. Panel C shows a typical fluorescence image of a 300 µm by 300 µm area taken with the ILEM in FM mode, and a zoom of the boxed area acquired in TEM mode. The sample was a thin plastic section of rat duodenum in which the mucous granule fields of goblet cells were fluorescently labeled with Alexa Fluor 488 conjugated wheat germ agglutinin. The optical module of the LSFM (panel D) was designed to fit in the limited space available in the TEM column and to be vacuum compatible. For this reason, the objective consists of a single aspherical lens, shielded from the rest of the optical system by a thin, flat vacuum window. The fluorescence emission is detected by an avalanche photo diode (APD). (With thanks to dr. Sasha Agronskaia for help with the recording of the fluorescence image in panel C.)

1.1.2.6. CLEM and Cryo-Electron Microscopy

Electron microscopists working in the life sciences have always been concerned with possible side-effects of chemical fixation, dehydration, embedding, and contrasting, on the ultrastructural preservation of tissues, cells, or isolated macromolecular complexes (see for example Murk et al., 2003). Thus the question arises, to what extent do the structural and molecular interactions observed in heavily processed specimens reflect the functioning in living cells. Cryo-electron microscopy emerged out of an urge to address this question (Lucic et al., 2005; McIntosh, 2001). Central to cryo-electron microscopic techniques is the preservation of biological specimens in their native, i.e. hydrated, state. This is achieved via vitrification, which has been discussed in section 1.3.3.1.

There is a price to be paid when studying biological samples in their native state. First of all, samples need to remain cooled at all times after vitrification to avoid ice crystal formation, which will occur if the temperature rises to -135 °C or higher (Al-Amoudi et al., 2004). This requires highly specialized equipment and techniques for handling and imaging. Secondly, cryo-EM images display a decreased signal-to-noise ratio due to the lack of image contrast. The reason for this is that the samples cannot be stained, and that they can only be viewed under low electron-dose conditions in order to avoid radiation damage. Thirdly, when the specimen thickness reaches ~600 nm or above, it cannot be observed anymore by a regular TEM. This restriction can be overcome by cutting ultrathin vitreous sections of the objects that are too large for direct observation (Al-Amoudi et al., 2004). This approach, termed CEMOVIS for cryo-electron microscopy of vitreous sections, adds to the complexity and required skills of the whole sample preparation procedure. Despite all the limitations mentioned here, several laboratories around the world perform cryo-EM and CEMOVIS routinely and successfully (Pierson et al., 2011; Zuber et al., 2005). Because of the complications and sectioning artifacts that result from vitreous sectioning, alternative techniques to thin down vitreous samples are also slowly arising. One of the most promising ones is FIB milling, in which a focused gallium ion beam is used to ablate the surface of a sample. The ion beam does not compromise the vitreous state of the sample, and the first FIB-thinned biological samples have been examined by cryo-EM and cryo-electron tomography (Hayles et al., 2010; Marko et al., 2007; Rigort et al., 2010).

Cryo-EM in cell biology is most rewarding when combined with tomography. Cryo-electron tomography allows for the 3D imaging of cellular components in a close-to-native state, with a resolution of 4 to 5 nanometers, high enough to detect macromolecular complexes (Grunewald et al., 2003; Steven and Aebi, 2003). There is increasing awareness that many of a cell's molecules are organized in larger macromolecular complexes or machines (Chiu et al., 2006; Nogales and Grigorieff, 2001), of which the ribosome is the quintessential example (Medalia et al., 2002); other examples are the nuclear pore complex (Beck et al., 2007) and the proteasome (Nickell et al., 2009; Walz et al., 1998). One of the most exciting applications of cryo-electron tomography is

subtomogram averaging, where identical protein structures from various tomograms are recognized and averaged with the help of computational methods, to achieve a high-resolution density map of the protein (Briggs et al., 2009; Forster et al., 2005). X-ray structures of the proteins can subsequently be fitted to the density maps, to recognize conformational variabilities in relation to other structures in the tomogram.

The aforementioned low contrast conditions and low electron-dose requirements for cryo-EM make it particularly difficult to locate areas of interest. Quite frequently, one only knows if the selected areas are interesting after the final image is collected or tomogram is reconstructed. Therefore, there is a demand for cryo-CLEM procedures to facilitate the identification of structures of interest, and replace the ”search for a needle in a haystack” by a guided search.

In chapters four and five of this thesis, two workflows are described for cryo-CLEM. The technical challenge these studies faced was that the fluorescence microscopy needed to be performed on specimens kept below the devitrification temperature of -135 °C, while using optics that yield sufficient resolution to obtain subcellular detail. One method primarily focuses on a cryo-stage to perform FM on vitreous samples. The other uses the integrated light and electron microscope (ILEM; described in section 1.1.2.5.). The techniques are applied to complete cells (chapter 4 and 5), isolated organelles (chapter 5), and in vitro generated macromolecular complexes (chapter 6).

1.1.3. CLEM Probes

1.1.3.1. Genetic Fluorescent tags

GFP

The gene for GFP, which is a naturally occurring fluorescent protein, was isolated from the jellyfish Aequorea victoria (Prasher et al., 1992). GFP emits green light when illuminated with blue light. In the jellyfish, the blue light is generated upon the binding of Ca2+ ions to the luminescent protein, aequorin (Shimomura, 2005). In the laboratory, the blue light is generated by lasers, LEDs, mercury or xenon vapor lamps. Several mutants of GFP have been engineered that emit stronger fluorescence and at different wavelengths (Tsien, 2005).

In principle, the fluorescence of GFP could be used to photooxidize DAB (see section 1.1.3.3. However, this is currently a matter of debate in the literature. Because the GFP chromophore is buried inside the protein, it would due to the lack of an aqueous environment, not be able to generate sufficient free radicals for efficacious photoconversion of DAB (Gaietta et al., 2002; Mironov et al., 2000). On the other hand, Monosov et al. (1996) demonstrated that GFP targeted to peroxisomes in yeast cells was able to photooxidize DAB at sufficient levels to permit EM localization; and Grabenbauer et al. (2005) reported on an improved method for GFP-mediated photo-oxidation. The improvements of the method, which they termed GRAB for GFP Recognition After Bleaching, consisted in the reduction of background by quenching of autofluorescence and blocking of endogenous enzyme activities, and in the use of elevated oxygen content throughout the photooxidation reaction. Following up on the work of Grabenbauer, Meisslitzer-Ruppitsch et al. also showed DAB photoconversion of the GFP variants EGFP and YFP (Meisslitzer-Ruppitsch et al., 2008). To this date, and to the best of our knowledge, only the three studies mentioned here have employed photooxidation by GFP. Meanwhile, alternative studies are developing GFP derivatives with more efficient production of singlet oxygen. Recently, Shu et al. (2011) introduced the protein ‘miniSOG’, for mini singlet oxygen generator. The probe is half the size of GFP, and the authors show it is capable of photoconverting DAB into its electron dense precipitate when bound to multiple cellular proteins, like actin, tubulin, and the proteins SynCAM1 and SynCAM2, which respectively localize to the pre- and postsynaptic membranes. An alternative correlative approach is to generate a fusion protein containing GFP as well as a tetracysteine motif (Gaietta et al., 2006). In this case, the GFP can be used for live cell imaging, whereas the tetracysteine motif (discussed below) can photooxidize DAB.

Tetracysteine tags

A tetra-cysteine (4C) motif is a small peptide sequence of 10-20 amino acids containing two pairs of cysteine residues that flank a pair of spacer amino acids (Cys-Cys-Xaa-Xaa-Cys-Cys, where Xaa represents a non-cysteine amino acid) (Giepmans et al., 2006; Tsien, 2005). This motif can

bind to fluorescent bi-arsenical derivatives, each arsenic interacting with one of the cysteine doublets. The most widely employed bi-arsenical dyes are the green-light emitting FlAsH (Fluorescein-based Arsenical Hairpin binder), and the red-light emitting ReAsH (Resorufin-based Arsenical Hairpin binder) (Machleidt et al., 2007; Tsien, 2005). These dyes are membrane-permeable and can therefore be used to label 4C tags in living cells (Gaietta et al., 2002; Gaietta et al., 2011a; Hoffmann et al., 2010; Rudner et al., 2005). Because arsenics are potentially cytotoxic, FlAsH and ReAsH need to be administered to the cells in combination with an antidote, such as 1,2-ethanedithiol or β-mercaptoethanol. In addition to reducing the toxicity of the bi-arsenical dyes, the antidote diminishes the fluorescence of the dyes prior to their binding to a 4C motif. Nevertheless, background fluorescence is an issue in this technique that can hamper the detection of weak signals. Part of this background fluorescence can be due to nonspecific binding of bi-arsenicals to endogenous proteins that are cysteine-rich (Stroffekova et al., 2001). Considerable effort has been directed towards optimizing the 4C/bi-arsenical labeling technique, and the future is likely to hold further improvements. Already new biarsenical probes have been devised that produce less background, and novel 4C motifs have been found that display higher affinity and stronger fluorescence (Adams et al., 2002; Martin et al., 2005; Spagnuolo et al., 2006).

Gaietta et al. (2002; 2011b) showed that ReAsH bound to tetra-cysteine motifs and immobilized by chemical fixation was able to photo-convert DAB (for a description of the method of DAB photooxidation, see section 1.1.3.3.). This technique allowed the authors to demonstrate differences in the intracellular trafficking route during mitosis between newly synthesized and older connexins, which are the building blocks of gap junctions (Boassa et al., 2010; Sosinsky et al., 2003). A correlative approach of the 4C technique that bypasses the cytotoxic effects of biarsenicals is given by Gaietta et al. (2006). The authors generated a fusion protein of the Golgi membrane protein α-mannosidase II tagged with a fluorescent protein (GFP/CFP) as well as a tetracysteine motif. The fluorescent protein was primarily used for live cell imaging, whereas the tetracysteine motif was used for DAB photooxidation. Although such a fusion protein overcomes the use of biarsenicals on live cells, the size of the proteins also increases, which increases the risk of interfering with the function of the original protein.

1.1.3.2. Fluorescent-Electron dense probes

Alexa-gold probes

A fluorescent-electron dense probing method that received reasonable attention in the literature is to conjugate to the same antibody or antibody fragment both a fluorochrome and a gold particle. Early attempts to generate such a probe led to the notion that fluorescence is quenched by colloidal gold, presumably by FRET from the fluorochrome to the gold particle (Powell et al., 1998). Despite that, secondary antibodies with both a fluorochrome conjugate and 5 or 10 nm colloidal gold are still commercially available. Kandela and Albrecht recently demonstrated that these are actually a mixture of antibodies carrying either fluorochromes only or both fluochromes and colloidal gold. They showed that the fluorescence of the colloidal gold conjugated antibodies was almost completely quenched (Kandela and Albrecht, 2007). These probes are therefore not suitable for a 1:1 colocalization as is ideally required for correlation between LM and EM, especially when taking into account the difference in penetration rate between antibodies with and without a gold label. Kandela et al. (2008) went on to show that the problem of fluorescence quenching can be overcome by separating the EM label and the LM label by a secondary antibody. In this case, a gold particle is coupled to the primary antibody, and a Cy3 molecule to the secondary antibody. The size of the gold particles should be kept small. For performing multiple labeling, they therefore suggest to use different metals for EM labeling, instead of different sizes of gold particles, and distinguish the metals by energy filtering TEM (Kandela et al., 2007).

Fluoronanogold

Another way to overcome fluorescence quenching by gold is by using small gold cluster complexes, i.e. nanogold, instead of colloidal gold (Robinson and Vandre, 1997). Due to the smaller size of the gold, there is an additional advantage, namely that the probe can penetrate cells and tissues more readily. The accessibility of antigenic sites to FluoroNanogold probes is further increased by coupling the fluorochrome and nanogold to only that portion of an antibody (the Fab' fragment) that binds to the antigen. However, nanogold particles are too small and display too little contrast to be observed by EM at the normal magnification range for heavy-metal stained biological specimens. An enlargement step is therefore required to increase the size and contrast of the gold particles. This can be achieved either by gold toning or by silver enhancement (Baschong and Stierhof, 1998; Sawada and Esaki, 2000). Both techniques are prone to artifacts, ranging from ultrastructural modifications to nonspecific precipitations (Baschong and Stierhof, 1998). They also eliminate the fluorescence properties of the fluorochrome, so that the fluorescence microscopy needs to be performed prior to the enlargement step. It is possible, however, to view the silver-enhanced immunogold signal by means of brightfield LM, thus allowing for precise correlation between the fluorescence and electron microscopic images. Notwithstanding the pitfalls associated with the use of FluoroNanogold, a number of studies have

emphasized its potential for CLEM applications. Most notably, Takizawa and Robinson (2003) applied FluoroNanogold to ultrathin cryosections of human placental tissue and were thus able to investigate by CLEM the subcellular distribution of markers of caveolae and endosomes.

Quantum dots

Quantum Dots (QDs) are inorganic, fluorescent semiconductor nanocrystals. They possess unique properties that are extremely advantageous for biomedical applications in general, and CLEM in particular: i) QDs can be tuned to emit light at a wide spectrum of wavelengths by changing their composition and size; ii) in comparison with organic fluorophores, QDs possess a long Stokes shift and a narrow emission spectrum, thus allowing for superior spectral separation and improved detection sensitivity; iii) QDs of different emission wavelengths can be excited by the same excitation wavelength, which facilitates imaging of multiple labels; iv) QDs have very high brightness owing to their extinction coefficient, which is at least ten times larger than that of the best dyes. This facilitates the imaging of individual QDs, and thus also single molecules, with high signal-to-noise-ratio (for a review, see Pinaud et al., 2010) v) unlike organic fluorophores, QDs can be illuminated over extended periods of time without showing any noticeable photobleaching; vi) because they are inorganic, QDs are resistant to biodegradation, and can therefore be used for in vivo imaging over extended periods of time; vii) QDs are electron dense and their sizes are within the range of immunogold particles, so that they can be detected by EM (Bruchez, 2005; Giepmans et al., 2005; Jaiswal and Simon, 2004; Larson et al., 2003; Nisman et al., 2004).

QDs are rapidly finding applications in many areas, ranging from nanotechnology to consumer electronics. The composition of QDs varies accordingly, and many laboratories are working on new and improved flavors. QDs that are employed in fluorescent probes typically possess a core-shell structure, the core consisting of cadmium selenide (CdSe), and the shell of zinc sulfide (ZnS). This core-shell configuration results in enhanced quantum yield and photostability. The size of the core determines the wavelength of the emitted light. Without modifications, QDs are toxic and hydrophobic, properties that are incompatible with studies in living cells, tissues or whole organisms, and that render difficult their conjugation to biomolecules. Therefore, QDs for biomedical research are often encapsulated with biocompatible surface coatings to prevent leaking of the toxic metals. Nevertheless, the potential toxic effects of QDs remain an area of concern amongst many investigators (Chang et al., 2006; Hardman, 2006; Ryman-Rasmussen et al., 2007).

QDs have been used and are commercially available as conjugates with secondary antibodies or streptavidin for indirect detection methods, but they can also be labeled directly to the functionalized biomolecules to permit binding of a molecule of interest (Michalet et al., 2005). The biologically reactive substances can sometimes cause the QDs to take on nonspecific interactions, against which another coating layer of polymers is often necessary (Liu et al., 2008).

All the surface coatings increase the size of QDs considerably, which may perturb the behavior of the labeled molecules (Brown and Verkade, 2010; Groc et al., 2007). Recent studies are therefore undertaken to reduce the thickness of coatings (Liu et al., 2008; Susumu et al., 2007).

Due to their size and properties, QDs cannot traverse the membrane of cells, thus limiting their usefulness for live cell imaging. It is therefore a challenge for current research to devise protocols that allow passage of QDs across the membrane of living cells (for a review, see Delehanty et al., 2009). An interesting mechanism is to conjugate QDs to intracellular signaling peptides. Hoshino et al. (2004) demonstrated that peptide sequences that encode either a nuclear localization signal or a mitochondrial localization signal, are rapidly targeted to nuclei or mitochondria, respectively, of cells in culture. The peptides cause the QDs to penetrate the cell membranes directly, thus via endocytosis-independent pathways (Liu et al., 2011). Also transfection reagents or biodegradable polymeric capsules encapsulating QDs can deliver QDs into the cytoplasm (Kim et al., 2008; Yoo et al., 2008). Another strategy involves the uptake of QDs via endocytosis, allowing for instance to monitor the dynamics of receptor internalization (Chang et al., 2006; Genovesio et al., 2006; Michalet et al., 2005; Seleverstov et al., 2006; Sundara Rajan and Vu, 2006). Duan and Nie (2007) reported that a surface coating of QDs with polyethylene glycol grafted polyethylimine allows the QDs to escape from endosomes via endosomolysis. Although it is a stretch to name these QDs ‘cell-penetrating’, they represent promising candidates for intracellular delivery of QDs. Further data will be needed to assess their cytotoxicity and their ability to be stably conjugated to biological detection molecules such as antibodies.

1.1.3.3. The DAB precipitation Method

The DAB method is based on the principle of DAB oxidation by free oxygen radicals. The free radicals can be formed during the enzymatic conversion of peroxide by horseradish peroxidase (HRP), or during photobleaching of fluorochromes by means of intense illumination and with oxygen present. When DAB is oxidized, it polymerizes and precipitates at the site of oxidation. The osmiophilic DAB precipitate becomes electron dense when treated with osmium tetroxide, and can thus be visualized by EM (Hanker, 1979; Maranto, 1982). The use of DAB photooxidation in CLEM experiments was recently reviewed by Meisslitzer-Ruppitsch et al. (2009).

Photooxidation appears to yield the best results when the DAB precipitation is confined to a fully or partially membrane-enclosed space, such as the lumen of a Golgi cisterna, a synaptic vesicle, or a dendritic spine (Capani et al., 2001; Darcy et al., 2006; Grabenbauer et al., 2005). Due to the nature of the reaction, the DAB staining is rather diffuse. As a consequence there is limited high-resolution information available in DAB labeled structures.

Horse Radish Peroxidase (HRP) is an alternative method to DAB photooxidation, and can be used to reveal fluorescent antibodies or GFP at the EM level. In the case of fluorescent antibodies, the primary antibodies are in turn detected by HRP-conjugated secondary antibodies. The HRP can afterwards convert DAB upon exposure to hydrogen peroxide, to create the electron dense precipitate. In the case of GFP, GFP epitopes are detected by GFP-antibodies that in turn are decorated by HRP-conjugated secondary antibodies (Mironov et al., 2000; Mironov et al., 2005). The GFP-HRP approach has been used successfully to identify and characterize transport intermediates along the secretory pathway (Polishchuk et al., 2000). Instead of labeling with the HRP protein, it is also possible to genetically conjugate the HRP gene to create a fusion-protein. After chemical fixation of cells expressing HRP, the cell permeable DAB can precipitate at the HRP-labeled sites. Since the precipitate can be visualized by LM as well as EM, this tool is also suitable for CLEM (Schikorski, 2010).

1.2. Cell Biological Problems Addressed in this Thesis

As illustrated by the considerable diversity in existing CLEM techniques described in section 1.1 of this Introduction, different cell biological questions require different CLEM approaches. The work presented in this thesis aimed at covering a wide variety of cell biological problems so that various CLEM techniques could be developed, improved, and applied.

Chapter 2: Diagnostic CLEM on tissue samples

In chapter 2, two diagnostically relevant samples were examined. Both consisted of patient material, i.e. tissue biopsies that were chemically fixed immediately following excision. The first one contained skeletal muscle tissue from a presymptomatic carrier of oculopharyngeal muscular dystrophy, a disease that is characterized electron microscopically by morphological changes of, among other things, the muscle nuclei. By fluorescently labeling the DNA in ultrathin TEM sections of this sample, FM could be used to generate an overview of the tissue and subsequent TEM correlation confirmed that in this patient the disease had not (yet) revealed itself. The second diagnostic sample was a tissue sample of an abdominal aortic aneurysm. Such an aneurysm is characterized histopathologically by large changes is the tunica media and intima of the artery wall, which brings about an inflammatory response. Using the same DNA labeling method as for the muscular tissue, it was possible to discriminate between different kinds of cells in ultrathin EM sections based on their fluorescence pattern. In particular neutrophils that infiltrate the inflamed area were readily identified within the panoply of cell types, because of their characteristic multilobed nuclei.

These examples illustrate how CLEM can complement diagnostic EM techniques as a means to facilitate the search in biopsies for areas of disease that require ultrastructural analysis. Thus at the LM level tissue samples can be surveyed to obtain rapidly relevant information on the orientation, architecture, and location of tissue components. It is then a matter of selecting areas of interest, which can be zoomed into at the EM level.

Although the diagnostic use of TEM has considerably diminished due to the advent of molecular biological tests (Biel and Gelderblom, 1999), there are still numerous clinically important diseases where EM excels as a diagnostic tool. These include skin and renal diseases involving structural defects of components of the extracellular matrix, in particular collagen; ciliary disorders such as Kartagener's syndrome where dynein arms and other components of the axoneme are absent or defective; lysosomal storage diseases; and pulmonary conditions caused by intrapulmonary deposits, especially asbestos (Howell et al., 1998; Carlen and Stenram, 2005; Foster et al., 2005; Suzuki et al., 2005; Alroy and Ucci, 2006). Diagnostic EM is also a vital and powerful tool for the identification of infectious agents such as viruses (Curry A et al, 2006; Schramlova et al., 2010). When combined with a negative stain procedure, it is a more rapid method for viral diagnosis than

other diagnostic tests that are currently available (Biel and Gelderblom, 1999). Moreover, and in contrast to other tests, diagnostic EM does not require any prior assumptions about the nature of the infectious agent, so that even unexpected pathogens can be detected, as well as multiple infections. It is this same undirectedness that renders TEM also important as a tool for assessing tumor cell lineage in the course of tumor diagnosis. Examples of ultrastructural determinants for cell lineage are Birbeck granules (Langerhans cells), lamellar bodies (alveolar epithelial type II cells), Weibel-Palade bodies (endothelial cells), and intercellular junctions (epithelial cells). By complementing diagnostic EM with LM, these structures can be identified more rapidly, and larger areas can be screened to increase the chance of identifying structures that are rare, and result in a more reliable diagnosis.

Other diagnostic EM applications that can benefit from a CLEM approach are the detection of thin basement membrane nephropathy and X-linked Alport syndrome. Both are glomerular disorders that are characterized by diffuse thinning of the glomerular basement membrane. Ultrastructural examination of renal biopsies is considered an essential step towards the final diagnosis of these diseases. However, the thickness of the glomerular basement membrane varies greatly and to obtain accurate measurements, care must be taken that the methods for tissue preparation and morphometry are standardized. For instance, it is common practice to measure the thickness of the basement membrane in at least 2 glomeruli and at random sites in different capillary loops with the same orientation (Foster et al., 2005). It would be much less time-consuming, if the selection of areas to be measured could be done at the LM level.

Chapter 2 describes yet more possible applications of the on-section CLEM approach for diagnostic TEM. In particular, these will include thin sections of complex tissues in which a certain area or structure is searched for. For example, after a DNA staining, samples can be screened for cells that are in a particular stage of mitosis. Chapter 2 also illustrates that, by using a lectin stain, the Golgi complex of intestinal goblet cells can be located in tissue samples of rat intestinal tissue. Although these large cells have an elaborate Golgi complex, due to different orientations of goblet cells in tissue sections it is very difficult to find sagittal sections in which the complete architecture of the Golgi apparatus is revealed.

Chapter 3: The complexity of Weibel-Palade body exocytosis

Chapter three elaborates on the process of regulated exocytosis of Weibel-Palade bodies from endothelial cells. Weibel-Palade bodies (WPBs) are storage granules of endothelial cells that release their contents into the blood flow in response to various physiological stimuli such as injury to the blood vessel wall, local inflammatory signals or hypoxia. The main constituent of WPBs, von Willebrand Factor (VWF), is a protein that is polymerized into long helical tubules, which give the WPBs their characteristic cigar shape. Following stimulation, the VWF becomes secreted into the blood flow where it forms long filaments that bind to exposed collagen and sequester platelets, thereby initiating the formation of a hemostatic plug.

The process of regulated exocytosis of WPBs is a highly controlled and complex process, which can adopt several forms: from full-granule collapse (i.e. classic or 'textbook' exocytosis) to the selective release of small proteins in a process called kiss-and-run exocytosis. Although major advances have been made in the elucidation of the molecular mechanisms governing regulated exocytosis, the process is still not completely understood. To give but one example, it remains to be established by which mechanism a secretory vesicle becomes destined for either full-collapse or kiss-and-run exocytosis.

During the study of VWF exocytosis by FM, large and spherical VWF-positive structures were found to appear in human umbilical vein endothelial cells (HUVECs). These structures were too large to be accounted for by the rounding up of single WPBs, and suggested a more complex mechanism of homotypic WPB fusion prior to exocytosis. Two CLEM approaches were used to characterize the unconventional exocytosis events detected by FM. Firstly, correlative FM and TEM were employed to obtain ultrastructural information of the VWF spheres, and secondly, correlative FM and SEM were used to identify sites of VWF exocytosis on the cell surface. The CLEM experiments provided important novel information on the exocytosis of VWF, and allowed us to propose that a significant proportion of WPBs engages in a process of multigranular exocytosis. This process was characterized by the coalescence of WPBs into large intracellular structures that we termed 'secretory pods'.

Chapter 4: The ultrastructure of unfixed, unsectioned mitochondria

In curiosity-driven studies of cellular processes, cultured cells are often used as a model system. This can be single-cell organisms such as bacteria or yeast, but also cells taken from larger organisms like mammals, and cultured in vitro. While bacteria are commonly thin enough throughout the cell to perform cryo-EM, certain cultured mammalian cells have a 'fried egg' appearance where the cell periphery is thin enough for cryo-EM. Indeed, the periphery of some cell types can be as thin as 50 nm (Koning et al., 2008). Mammalian cell types that have until now been studied under cryo-EM conditions are for example HUVECs (Berriman et al., 2009), fibroblasts (Koning et al., 2008; Maurer et al., 2008), Glioblastoma cells (Carlson et al., 2010), keratinocytes (Sartori et al., 2007), neurons (Lucic et al., 2007), and more (for a review, see Koning and Koster, 2009).

Together, these studies have demonstrated that cells can be studied not only in a near-native state, but also without the need for sectioning. Structural features can therefore be observed while intact, so that a more 3-dimensional view can be deducted from tomograms. On the other hand, it remains challenging to locate specific structures by visual inspection in cryo-EM. In this chapter, we designed a cryo-CLEM approach that facilitated the localization of labeled structures, to subsequently perform cryo-electron tomography on the nonsectioned material. As a proof of principal, we imaged whole mitochondria in HUVECs, and were able to show that the mitochondrial cristae in these cells connect to the intermembrane space via relatively large slits.

This finding contrasts with the current view that mitochondrial cristae connect to the intermembrane space via small pores whose size may modulate the diffusion of metabolites. A logical consequence of the whole-cell cryo-CLEM technique is that the structures under study have to be located in thin (regions of) cells. It may therefore not be suitable for studies in thicker cells or cell areas. However, examples of biological applications for which the whole cell cryo-CLEM approach would be suitable include virus budding events, microtubule plus-end dynamics, vesicle transport along the cytoskeleton, and synaptic vesicle exocytosis. For structures or events that take place in thicker (regions of) cells, a step of vitreous sectioning needs to precede cryo-CLEM (see chapter 6).

Chapter 5: Role of actin coated granules (ACGs) during regulated exocytosis

One of the main reasons to perform CLEM is when the biological events under study are so short-lived that they are captured only rarely in static EM preparations. LM functions in this case to localize the events in a low magnification overview. An example of such an event is actin coating of secretory granules during their regulated exocytosis. Actin coating occurs after stimulation of exocytosis, and has been observed in multiple models of regulated exocytosis, such as oocytes, lacrimal cells, alveolar epithelial type II cells, and pancreatic acinar cells. The functional significance of actin coating of secretory granules is still not fully understood, and it remains a matter of debate whether actin coating occurs prior to or subsequent to the membrane fusion event. Owing to the rarity of actin coating events, most-likely due to their short-livedness, EM observations have never been made (Valentijn et al., 2000).

Chapter 5 discusses work in progress to use cryo-CLEM for the localization of ACGs in tissue homogenates of rat pancreas. Formation of ACGs was induced in vitro by the addition of GTPγS. Our work so far demonstrates the power of cryo-CLEM combined with cryo-electron tomography to obtain high-resolution information of rare events in their native state. Unfortunately, intact zymogen granules tended to form clusters that were too thick for tomography. For the ultrastructural characterization of the actin coats, we therefore focused on zymogen granules that were damaged and whose contents were partially released, but that still displayed an actin coat.

Chapter 6: Smaller features and weaker fluorescence: from super-resolution LM to ultrathin vitreous sections

This chapter explores the state-of-the-art and future of CLEM and cryo-CLEM; what can be achieved with current techniques, and how can they be improved in the future? Also included are latest results from cryo-methods on the cutting edge of CLEM.

References

Adams, S.R., R.E. Campbell, L.A. Gross, B.R. Martin, G.K. Walkup, Y. Yao, J. Llopis, and R.Y. Tsien, 2002. New biarsenical ligands and tetracysteine motifs for protein labeling in vitro and in vivo: synthesis and biological applications. J Am Chem Soc 124: 6063-76.

Agronskaia, A.V., J.A. Valentijn, L.F. van Driel, C.T. Schneijdenberg, B.M. Humbel, P.M. van Bergen en Henegouwen, A.J. Verkleij, A.J. Koster, and H.C. Gerritsen, 2008. Integrated fluorescence and transmission electron microscopy. J Struct Biol 164: 183-9.

Al-Amoudi, A., J.J. Chang, A. Leforestier, A. McDowall, L.M. Salamin, L.P. Norlen, K. Richter, N.S. Blanc, D. Studer, and J. Dubochet, 2004. Cryo-electron microscopy of vitreous sections. EMBO J 23: 3583-8.

Andresen, M., R. Schmitz-Salue, and S. Jakobs, 2004. Short tetracysteine tags to beta-tubulin demonstrate the significance of small labels for live cell imaging. Mol Biol Cell 15: 5616-22.

Armer, H.E., G. Mariggi, K.M. Png, C. Genoud, A.G. Monteith, A.J. Bushby, H. Gerhardt, and L.M. Collinson, 2009. Imaging transient blood vessel fusion events in zebrafish by correlative volume electron microscopy. PLoS One 4: e7716.

Bao, G., W.J. Rhee, and A. Tsourkas, 2009. Fluorescent probes for live-cell RNA detection. Annu Rev Biomed Eng 11: 25-47.

Baschong, W., and Y.D. Stierhof, 1998. Preparation, use, and enlargement of ultrasmall gold particles in immunoelectron microscopy. Microsc Res Tech 42: 66-79.

Beck, M., V. Lucic, F. Forster, W. Baumeister, and O. Medalia, 2007. Snapshots of nuclear pore complexes in action captured by cryo-electron tomography. Nature 449: 611-5.

Berriman, J.A., S. Li, L.J. Hewlett, S. Wasilewski, F.N. Kiskin, T. Carter, M.J. Hannah, and P.B. Rosenthal, 2009. Structural organization of Weibel-Palade bodies revealed by cryo-EM of vitrified endothelial cells. Proc Natl Acad Sci U S A 106: 17407-12.

Biel, S.S., K. Kawaschinski, K.P. Wittern, U. Hintze, and R. Wepf, 2003. From tissue to cellular ultrastructure: closing the gap between micro- and nanostructural imaging. J Microsc 212: 91-9.

Boassa, D., J.L. Solan, A. Papas, P. Thornton, P.D. Lampe, and G.E. Sosinsky, 2010. Trafficking and recycling of the connexin43 gap junction protein during mitosis. Traffic 11: 1471-86.

Braet, F., E. Wisse, P. Bomans, P. Frederik, W. Geerts, A. Koster, L. Soon, and S. Ringer, 2007. Contribution of high-resolution correlative imaging techniques in the study of the liver sieve in three-dimensions. Microsc Res Tech 70: 230-42.

Briggs, J.A., J.D. Riches, B. Glass, V. Bartonova, G. Zanetti, and H.G. Krausslich, 2009. Structure and assembly of immature HIV. Proc Natl Acad Sci U S A 106: 11090-5.

Brown, E., and P. Verkade, 2010. The use of markers for correlative light electron microscopy. Protoplasma 244: 91-7.

Brown, E., J. Mantell, D. Carter, G. Tilly, and P. Verkade, 2009. Studying intracellular transport using high-pressure freezing and Correlative Light Electron Microscopy. Semin Cell Dev Biol 20: 910-9.

Bruchez, M.P., 2005. Turning all the lights on: quantum dots in cellular assays. Curr Opin Chem Biol 9: 533-7.

Buckley, I.K., 1971. A simple technique for comparative light and electron microscopy of designated living cultured cells. Lab Invest 25: 295-301.

Capani, F., T.J. Deerinck, M.H. Ellisman, E. Bushong, M. Bobik, and M.E. Martone, 2001. Phalloidin-eosin followed by photo-oxidation: a novel method for localizing F-actin at the light and electron microscopic levels. J Histochem Cytochem 49: 1351-61.

Carlson, L.A., A. de Marco, H. Oberwinkler, A. Habermann, J.A. Briggs, H.G. Krausslich, and K. Grunewald, 2010. Cryo electron tomography of native HIV-1 budding sites. PLoS Pathog 6: e1001173.

Chalfie, M., Y. Tu, G. Euskirchen, W.W. Ward, and D.C. Prasher, 1994. Green fluorescent protein as a marker for gene expression. Science 263: 802-5.

Chang, W.H., W.Y. Chen, H.S. Chang, T.P. Hsieh, J.I. Chyi, and T.M. Hsu, 2006. Efficient single-photon sources based on low-density quantum dots in photonic-crystal nanocavities. Phys Rev Lett 96: 117401.

Chiu, W., M.L. Baker, and S.C. Almo, 2006. Structural biology of cellular machines. Trends Cell Biol 16: 144-50.

Cochilla, A.J., J.K. Angleson, and W.J. Betz, 1999. Monitoring secretory membrane with FM1-43 fluorescence. Annu Rev Neurosci 22: 1-10.

Coleman, R.A., J. Liu, and J.B. Wade, 2006. Use of anti-fluorophore antibody to achieve high-sensitivity immunolocalizations of transporters and ion channels. J Histochem Cytochem 54: 817-27.

Costello, M.J., 2006. Cryo-electron microscopy of biological samples. Ultrastruct Pathol 30: 361-71.

Darcy, K.J., K. Staras, L.M. Collinson, and Y. Goda, 2006. Constitutive sharing of recycling synaptic vesicles between presynaptic boutons. Nat Neurosci 9: 315-21.

Das, S.C., D. Panda, D. Nayak, and A.K. Pattnaik, 2009. Biarsenical labeling of vesicular stomatitis virus encoding tetracysteine-tagged m protein allows dynamic imaging of m protein and virus uncoating in infected cells. J Virol 83: 2611-22.

De Winter, D.A., C.T. Schneijdenberg, M.N. Lebbink, B. Lich, A.J. Verkleij, M.R. Drury, and B.M. Humbel, 2009. Tomography of insulating biological and geological materials using focused ion beam (FIB) sectioning and low-kV BSE imaging. J Microsc 233: 372-83.

Delehanty, J.B., H. Mattoussi, and I.L. Medintz, 2009. Delivering quantum dots into cells: strategies, progress and remaining issues. Anal Bioanal Chem 393: 1091-105.

Denk, W., and H. Horstmann, 2004. Serial block-face scanning electron microscopy to reconstruct three-dimensional tissue nanostructure. PLoS Biol 2: e329.

Duan, H., and S. Nie, 2007. Cell-penetrating quantum dots based on multivalent and endosome-disrupting surface coatings. J Am Chem Soc 129: 3333-8.

Dubochet, J., M. Adrian, J.J. Chang, J.C. Homo, J. Lepault, A.W. McDowall, and P. Schultz, 1988. Cryo-electron microscopy of vitrified specimens. Q Rev Biophys 21: 129-228.

Evans, W.H., and P.E. Martin, 2002. Lighting up gap junction channels in a flash. Bioessays 24: 876-80.

Fairen, A., 2005. Pioneering a golden age of cerebral microcircuits: the births of the combined Golgi-electron microscope methods. Neuroscience 136: 607-14.

Forster, F., O. Medalia, N. Zauberman, W. Baumeister, and D. Fass, 2005. Retrovirus envelope protein complex structure in situ studied by cryo-electron tomography. Proc Natl Acad Sci U S A 102: 4729-34.

Frischknecht, F., O. Renaud, and S.L. Shorte, 2006. Imaging today's infectious animalcules. Curr Opin Microbiol 9: 297-306.

Gaietta, G., T.J. Deerinck, S.R. Adams, J. Bouwer, O. Tour, D.W. Laird, G.E. Sosinsky, R.Y. Tsien, and M.H. Ellisman, 2002. Multicolor and electron microscopic imaging of connexin trafficking. Science 296: 503-7.

Gaietta, G.M., T.J. Deerinck, and M.H. Ellisman, 2011a. Correlated live cell light and electron microscopy using tetracysteine tags and biarsenicals. Cold Spring Harb Protoc 2011: pdb top94.

Gaietta, G.M., T.J. Deerinck, and M.H. Ellisman, 2011b. Fluorescence Photoconversion of Biarsenical-Labeled Cells for Correlated Electron Microscopy (EM). Cold Spring Harb Protoc 2011: pdb prot5548.

Gaietta, G.M., B.N. Giepmans, T.J. Deerinck, W.B. Smith, L. Ngan, J. Llopis, S.R. Adams, R.Y. Tsien, and M.H. Ellisman, 2006. Golgi twins in late mitosis revealed by genetically encoded tags for live cell imaging and correlated electron microscopy. Proc Natl Acad Sci U S A 103: 17777-82.

Genovesio, A., T. Liedl, V. Emiliani, W.J. Parak, M. Coppey-Moisan, and J.C. Olivo-Marin, 2006. Multiple particle tracking in 3-D+t microscopy: method and application to the tracking of endocytosed quantum dots. IEEE Trans Image Process 15: 1062-70.

Geuze, H.J., 1999. A future for electron microscopy in cell biology? Trends Cell Biol 9: 92-3.

Giddings, T.H., 2003. Freeze-substitution protocols for improved visualization of membranes in high-pressure frozen samples. J Microsc 212: 53-61.

Giepmans, B.N., S.R. Adams, M.H. Ellisman, and R.Y. Tsien, 2006. The fluorescent toolbox for assessing protein location and function. Science 312: 217-24.

Giepmans, B.N., T.J. Deerinck, B.L. Smarr, Y.Z. Jones, and M.H. Ellisman, 2005. Correlated light and electron microscopic imaging of multiple endogenous proteins using Quantum dots. Nat Methods 2: 743-9.

Glauert, A.M., 1974. The high voltage electron microscope in biology. J Cell Biol 63: 717-48.

Grabenbauer, M., W.J. Geerts, J. Fernadez-Rodriguez, A. Hoenger, A.J. Koster, and T. Nilsson, 2005. Correlative microscopy and electron tomography of GFP through photooxidation. Nat Methods 2: 857-62.

Groc, L., M. Lafourcade, M. Heine, M. Renner, V. Racine, J.B. Sibarita, B. Lounis, D. Choquet, and L. Cognet, 2007. Surface trafficking of neurotransmitter receptor: comparison between single-molecule/quantum dot strategies. J Neurosci 27: 12433-7.

Groos, S., E. Reale, and L. Luciano, 2001. Re-evaluation of epoxy resin sections for light and electron microscopic immunostaining. J Histochem Cytochem 49: 397-406.

Grunewald, K., O. Medalia, A. Gross, A.C. Steven, and W. Baumeister, 2003. Prospects of electron cryotomography to visualize macromolecular complexes inside cellular compartments: implications of crowding. Biophys Chem 100: 577-91.

Guizetti, J., J. Mantler, T. Muller-Reichert, and D.W. Gerlich, 2010. Correlative time-lapse imaging and electron microscopy to study abscission in HeLa cells. Methods Cell Biol 96: 591-601.

Hanker, J.S., 1979. Osmiophilic reagents in electronmicroscopic histocytochemistry. Prog Histochem Cytochem 12: 1-85.

Hanson, D.A., and S.F. Ziegler, 2004. Fusion of green fluorescent protein to the C-terminus of granulysin alters its intracellular localization in comparison to the native molecule. J Negat Results Biomed 3: 2.

Hardman, R., 2006. A toxicologic review of quantum dots: toxicity depends on physicochemical and environmental factors. Environ Health Perspect 114: 165-72.

Hayat, M.A., 1987. Correlative Microscopy in Biology. Instrumentation and Methods. Academic Press, Inc., London.

Hayles, M.F., D.A. Matthijs de Winter, C.T. Schneijdenberg, J.D. Meeldijk, U. Luecken, H. Persoon, J. de Water, F. de Jong, B.M. Humbel, and A.J. Verkleij, 2010. The making of frozen-hydrated, vitreous lamellas from cells for cryo-electron microscopy. J Struct Biol 172: 180-90.

Hekking, L.H., M.N. Lebbink, D.A. De Winter, C.T. Schneijdenberg, C.M. Brand, B.M. Humbel, A.J. Verkleij, and J.A. Post, 2009. Focused ion beam-scanning electron microscope: exploring large volumes of atherosclerotic tissue. J Microsc 235: 336-47.

Heymann, J.A., M. Hayles, I. Gestmann, L.A. Giannuzzi, B. Lich, and S. Subramaniam, 2006. Site-specific 3D imaging of cells and tissues with a dual beam microscope. J Struct Biol 155: 63-73.

Hinner, M.J., and K. Johnsson, 2010. How to obtain labeled proteins and what to do with them. Curr Opin Biotechnol 21: 766-76.

Hoffmann, C., G. Gaietta, A. Zurn, S.R. Adams, S. Terrillon, M.H. Ellisman, R.Y. Tsien, and M.J. Lohse, 2010. Fluorescent labeling of tetracysteine-tagged proteins in intact cells. Nat Protoc 5: 1666-77.

Hohensee, S., W. Bleiss, and C. Duch, 2008. Correlative electron and confocal microscopy assessment of synapse localization in the central nervous system of an insect. J Neurosci Methods 168: 64-70.

Hollander, H., 1970. The section embedding (SE) technique. A new method for the combined light microscopic and electron microscopic examination of central nervous tissue. Brain Res 20: 39-47.

Hoshino, A., K. Fujioka, T. Oku, S. Nakamura, M. Suga, Y. Yamaguchi, K. Suzuki, M. Yasuhara, and K. Yamamoto, 2004. Quantum dots targeted to the assigned organelle in living cells. Microbiol Immunol 48: 985-94.

Howarth, M., W. Liu, S. Puthenveetil, Y. Zheng, L.F. Marshall, M.M. Schmidt, K.D. Wittrup, M.G. Bawendi, and A.Y. Ting, 2008. Monovalent, reduced-size quantum dots for imaging receptors on living cells. Nat Methods 5: 397-9.

Hyde, G.J., D.S. Davies, L. Cole, and A.E. Ashford, 2003. Retention of fluorescent probes during aldehyde-free anhydrous freeze-substitution. J Microsc 210: 125-30.

Jahn, K.A., D.A. Barton, Y. Su, J. Riches, E.P. Kable, L.L. Soon, and F. Braet, 2009. Correlative fluorescence and transmission electron microscopy: an elegant tool to study the actin cytoskeleton of whole-mount (breast) cancer cells. J Microsc 235: 282-92.

Jaiswal, J.K., and S.M. Simon, 2004. Potentials and pitfalls of fluorescent quantum dots for biological imaging. Trends Cell Biol 14: 497-504.

Jiao, W., A. Shupliakov, and O. Shupliakov, 2010. A semi-correlative technique for the subcellular localization of proteins in Drosophila synapses. J Neurosci Methods 185: 273-9.

Jimenez, N., E.G. Van Donselaar, D.A. De Winter, K. Vocking, A.J. Verkleij, and J.A. Post, 2010. Gridded Aclar: preparation methods and use for correlative light and electron microscopy of cell monolayers, by TEM and FIB-SEM. J Microsc 237: 208-20.

Jones, M.K., S.H. Bong, K.M. Green, P. Holmes, M. Duke, A. Loukas, and D.P. McManus, 2008. Correlative and dynamic imaging of the hatching biology of Schistosoma japonicum from eggs prepared by high pressure freezing. PLoS Negl Trop Dis 2: e334.

Jones, S., S.K. Chapman, P.R. Crocker, G. Carson, and D.A. Levison, 1982. Combined light and electron microscope in routine histopathology. J Clin Pathol 35: 425-9.

Kamioka, H., S.A. Murshid, Y. Ishihara, N. Kajimura, T. Hasegawa, R. Ando, Y. Sugawara, T. Yamashiro, A. Takaoka, and T. Takano-Yamamoto, 2009. A method for observing silver-stained osteocytes in situ in 3-microm sections using ultra-high voltage electron microscopy tomography. Microsc Microanal 15: 377-83.

Kandela, I.K., and R.M. Albrecht, 2007. Fluorescence quenching by colloidal heavy metals nanoparticles: implications for correlative fluorescence and electron microscopy studies. Scanning 29: 152-61.

Kandela, I.K., R. Bleher, and R.M. Albrecht, 2007. Multiple correlative immunolabeling for light and electron microscopy using fluorophores and colloidal metal particles. J Histochem Cytochem 55: 983-90.

Kandela, I.K., R. Bleher, and R.M. Albrecht, 2008. Immunolabeling for correlative light and electron microscopy on ultrathin cryosections. Microsc Microanal 14: 159-65.

Karreman, M.A., A.V. Agronskaia, A.J. Verkleij, F.F. Cremers, H.C. Gerritsen, and B.M. Humbel, 2009. Discovery of a new RNA-containing nuclear structure in UVC-induced apoptotic cells by integrated laser electron microscopy. Biol Cell 101: 287-99.

Keene, D.R., S.F. Tufa, G.P. Lunstrum, P. Holden, and W.A. Horton, 2008. Confocal/TEM overlay microscopy: a simple method for correlating confocal and electron microscopy of cells expressing GFP/YFP fusion proteins. Microsc Microanal 14: 342-8.

Keppler, A., S. Gendreizig, T. Gronemeyer, H. Pick, H. Vogel, and K. Johnsson, 2003. A general method for the covalent labeling of fusion proteins with small molecules in vivo. Nat Biotechnol 21: 86-9.

Kim, B.Y., W. Jiang, J. Oreopoulos, C.M. Yip, J.T. Rutka, and W.C. Chan, 2008. Biodegradable quantum dot nanocomposites enable live cell labeling and imaging of cytoplasmic targets. Nano Lett 8: 3887-92.

Knoops, K., M. Kikkert, S.H. Worm, J.C. Zevenhoven-Dobbe, Y. van der Meer, A.J. Koster, A.M. Mommaas, and E.J. Snijder, 2008. SARS-coronavirus replication is supported by a reticulovesicular network of modified endoplasmic reticulum. PLoS Biol 6: e226.

Kolotuev, I., Y. Schwab, and M. Labouesse, 2009. A precise and rapid mapping protocol for correlative light and electron microscopy of small invertebrate organisms. Biol Cell 102: 121-32.

Koning, R.I., and A.J. Koster, 2009. Cryo-electron tomography in biology and medicine. Ann Anat 191: 427-45.

Koning, R.I., S. Zovko, M. Barcena, G.T. Oostergetel, H.K. Koerten, N. Galjart, A.J. Koster, and A.M. Mommaas, 2008. Cryo electron tomography of vitrified fibroblasts: microtubule plus ends in situ. J Struct Biol 161: 459-68.

Koster, A.J., and J. Klumperman, 2003. Electron microscopy in cell biology: integrating structure and function. Nat Rev Mol Cell Biol Suppl: SS6-10.

Koster, A.J., R. Grimm, D. Typke, R. Hegerl, A. Stoschek, J. Walz, and W. Baumeister, 1997. Perspectives of molecular and cellular electron tomography. J Struct Biol 120: 276-308.

Kreplak, L., K. Richter, U. Aebi, and H. Herrmann, 2008. Electron microscopy of intermediate filaments: teaming up with atomic force and confocal laser scanning microscopy. Methods Cell Biol 88: 273-97.

Kukulski, W., M. Schorb, S. Welsch, A. Picco, M. Kaksonen, and J.A. Briggs, 2011. Correlated fluorescence and 3D electron microscopy with high sensitivity and spatial precision. J Cell Biol 192: 111-9.

Ladinsky, M.S., J.R. Kremer, P.S. Furcinitti, J.R. McIntosh, and K.E. Howell, 1994. HVEM tomography of the trans-Golgi network: structural insights and identification of a lace-like vesicle coat. J Cell Biol 127: 29-38.

Larson, D.R., W.R. Zipfel, R.M. Williams, S.W. Clark, M.P. Bruchez, F.W. Wise, and W.W. Webb, 2003. Water-soluble quantum dots for multiphoton fluorescence imaging in vivo. Science 300: 1434-6.

Leapman, R.D., 2004. Novel techniques in electron microscopy. Curr Opin Neurobiol 14: 591-8.

Liou, W., H.J. Geuze, and J.W. Slot, 1996. Improving structural integrity of cryosections for immunogold labeling. Histochem Cell Biol 106: 41-58.

Liu, B.R., Y.W. Huang, J.G. Winiarz, H.J. Chiang, and H.J. Lee, 2011. Intracellular delivery of quantum dots mediated by a histidine- and arginine-rich HR9 cell-penetrating peptide through the direct membrane translocation mechanism. Biomaterials 32: 3520-37.

Liu, W., M. Howarth, A.B. Greytak, Y. Zheng, D.G. Nocera, A.Y. Ting, and M.G. Bawendi, 2008. Compact biocompatible quantum dots functionalized for cellular imaging. J Am Chem Soc 130: 1274-84.

Los, G.V., L.P. Encell, M.G. McDougall, D.D. Hartzell, N. Karassina, C. Zimprich, M.G. Wood, R. Learish, R.F. Ohana, M. Urh, D. Simpson, J. Mendez, K. Zimmerman, P. Otto, G. Vidugiris, J. Zhu, A. Darzins, D.H. Klaubert, R.F. Bulleit, and K.V. Wood, 2008. HaloTag: a novel protein labeling technology for cell imaging and protein analysis. ACS Chem Biol 3: 373-82.

Luby-Phelps, K., G. Ning, J. Fogerty, and J.C. Besharse, 2003. Visualization of identified GFP-expressing cells by light and electron microscopy. J Histochem Cytochem 51: 271-4.

Lucic, V., F. Forster, and W. Baumeister, 2005. Structural studies by electron tomography: from cells to molecules. Annu Rev Biochem 74: 833-65.

Lucic, V., A.H. Kossel, T. Yang, T. Bonhoeffer, W. Baumeister, and A. Sartori, 2007. Multiscale imaging of neurons grown in culture: from light microscopy to cryo-electron tomography. J Struct Biol 160: 146-56.

Machleidt, T., M. Robers, and G.T. Hanson, 2007. Protein labeling with FlAsH and ReAsH. Methods Mol Biol 356: 209-20.

Manfredi, J.J., J. Parness, and S.B. Horwitz, 1982. Taxol binds to cellular microtubules. J Cell Biol 94: 688-96.

Maranto, A.R., 1982. Neuronal mapping: a photooxidation reaction makes Lucifer yellow useful for electron microscopy. Science 217: 953-5.

Marko, M., C. Hsieh, R. Schalek, J. Frank, and C. Mannella, 2007. Focused-ion-beam thinning of frozen-hydrated biological specimens for cryo-electron microscopy. Nat Methods 4: 215-7.

Marsh, B.J., 2005. Lessons from tomographic studies of the mammalian Golgi. Biochim Biophys Acta 1744: 273-92.

Martin, B.R., B.N. Giepmans, S.R. Adams, and R.Y. Tsien, 2005. Mammalian cell-based optimization of the biarsenical-binding tetracysteine motif for improved fluorescence and affinity. Nat Biotechnol 23: 1308-14.

Maurer, U.E., B. Sodeik, and K. Grunewald, 2008. Native 3D intermediates of membrane fusion in herpes simplex virus 1 entry. Proc Natl Acad Sci U S A 105: 10559-64.

McDonald, K.L., 2009. A review of high-pressure freezing preparation techniques for correlative light and electron microscopy of the same cells and tissues. J Microsc 235: 273-81.

McDonald, K.L., and M. Auer, 2006. High-pressure freezing, cellular tomography, and structural cell biology. Biotechniques 41: 137, 139, 141.

McEwen, B.F., and M. Marko, 2001. The emergence of electron tomography as an important tool for investigating cellular ultrastructure. J Histochem Cytochem 49: 553-64.

McEwen, B.F., A.B. Heagle, G.O. Cassels, K.F. Buttle, and C.L. Rieder, 1997. Kinetochore fiber maturation in PtK1 cells and its implications for the mechanisms of chromosome congression and anaphase onset. J Cell Biol 137: 1567-80.

McIntosh, J.R., 2001. Electron microscopy of cells: a new beginning for a new century. J Cell Biol 153: F25-32.

McIntosh, R., D. Nicastro, and D. Mastronarde, 2005. New views of cells in 3D: an introduction to electron tomography. Trends Cell Biol 15: 43-51.

McNary, W.F., Jr., R.C. Rosan, and J.A. Kerrigan, 1964. Flourescent Microscopy of Thin Sections as an Adjunct to Electron Microscopy. J Histochem Cytochem 12: 216-7.

Medalia, O., I. Weber, A.S. Frangakis, D. Nicastro, G. Gerisch, and W. Baumeister, 2002. Macromolecular architecture in eukaryotic cells visualized by cryoelectron tomography. Science 298: 1209-13.

Meisslitzer-Ruppitsch, C., C. Rohrl, J. Neumuller, M. Pavelka, and A. Ellinger, 2009. Photooxidation technology for correlated light and electron microscopy. J Microsc 235: 322-35.

Meisslitzer-Ruppitsch, C., M. Vetterlein, H. Stangl, S. Maier, J. Neumuller, M. Freissmuth, M. Pavelka, and A. Ellinger, 2008. Electron microscopic visualization of fluorescent signals in cellular compartments and organelles by means of DAB-photoconversion. Histochem Cell Biol 130: 407-19.

Michalet, X., F.F. Pinaud, L.A. Bentolila, J.M. Tsay, S. Doose, J.J. Li, G. Sundaresan, A.M. Wu, S.S. Gambhir, and S. Weiss, 2005. Quantum dots for live cells, in vivo imaging, and diagnostics. Science 307: 538-44.

Mironov, A.A., R.S. Polishchuk, and A. Luini, 2000. Visualizing membrane traffic in vivo by combined video fluorescence and 3D electron microscopy. Trends Cell Biol 10: 349-53.

Mironov, A.A., G.V. Beznoussenko, A. Luini, and R.S. Polishchuk, 2005. Visualizing intracellular events in vivo by combined video fluorescence and 3-D electron microscopy. Methods Enzymol 404: 43-57.

Monosov, E.Z., T.J. Wenzel, G.H. Luers, J.A. Heyman, and S. Subramani, 1996. Labeling of peroxisomes with green fluorescent protein in living P. pastoris cells. J Histochem Cytochem 44: 581-9.

Mori, M., G. Ishikawa, T. Takeshita, T. Goto, J.M. Robinson, and T. Takizawa, 2006. Ultrahigh-resolution immunofluorescence microscopy using ultrathin cryosections: subcellular distribution of caveolin-1alpha and CD31 in human placental endothelial cells. J Electron Microsc (Tokyo) 55: 107-12.

Morozov, Y., I. Khalilov, Y. Ben-Ari, and A. Represa, 2002. Correlative fluorescence and electron microscopy of biocytin-filled neurons with a preservation of the postsynaptic ultrastructure. J Neurosci Methods 117: 81-5.

Muller-Reichert, T., J. Mantler, M. Srayko, and E. O'Toole, 2008. Electron microscopy of the early Caenorhabditis elegans embryo. J Microsc 230: 297-307.

Muller-Reichert, T., M. Srayko, A. Hyman, E.T. O'Toole, and K. McDonald, 2007. Correlative light and electron microscopy of early Caenorhabditis elegans embryos in mitosis. Methods Cell Biol 79: 101-19.

Murk, J.L., G. Posthuma, A.J. Koster, H.J. Geuze, A.J. Verkleij, M.J. Kleijmeer, and B.M. Humbel, 2003. Influence of aldehyde fixation on the morphology of endosomes and lysosomes: quantitative analysis and electron tomography. J Microsc 212: 81-90.

Nelson, A.C., 1986. Computer-aided microtomography with true 3-D display in electron microscopy. J Histochem Cytochem 34: 57-60.

Newman, G.R., and J.A. Hobot, 1999. Resins for combined light and electron microscopy: a half century of development. Histochem J 31: 495-505.

Nickell, S., F. Beck, S.H. Scheres, A. Korinek, F. Forster, K. Lasker, O. Mihalache, N. Sun, I. Nagy, A. Sali, J.M. Plitzko, J.M. Carazo, M. Mann, and W. Baumeister, 2009. Insights into the molecular architecture of the 26S proteasome. Proc Natl Acad Sci U S A 106: 11943-7.

Nikonenko, I., B. Boda, S. Alberi, and D. Muller, 2005. Application of photoconversion technique for correlated confocal and ultrastructural studies in organotypic slice cultures. Microsc Res Tech 68: 90-6.

Nisman, R., G. Dellaire, Y. Ren, R. Li, and D.P. Bazett-Jones, 2004. Application of quantum dots as probes for correlative fluorescence, conventional, and energy-filtered transmission electron microscopy. J Histochem Cytochem 52: 13-8.

Nixon, S.J., R.I. Webb, M. Floetenmeyer, N. Schieber, H.P. Lo, and R.G. Parton, 2009. A single method for cryofixation and correlative light, electron microscopy and tomography of zebrafish embryos. Traffic 10: 131-6.

Nogales, E., and N. Grigorieff, 2001. Molecular Machines: putting the pieces together. J Cell Biol 152: F1-10.

Oberti, D., M.A. Kirschmann, and R.H. Hahnloser, 2010. Correlative microscopy of densely labeled projection neurons using neural tracers. Front Neuroanat 4: 24.

Oorschot, V., H. de Wit, W.G. Annaert, and J. Klumperman, 2002. A novel flat-embedding method to prepare ultrathin cryosections from cultured cells in their in situ orientation. J Histochem Cytochem 50: 1067-80.

Peters, A., 2002. Examining neocortical circuits: some background and facts. J Neurocytol 31: 183-93.

Peters, P.J., and J. Pierson, 2008. Immunogold labeling of thawed cryosections. Methods Cell Biol 88: 131-49.

Pfeiffer, S., M. Beese, M. Boettcher, K. Kawaschinski, and K. Krupinska, 2003. Combined use of confocal laser scanning microscopy and transmission electron microscopy for visualisation of identical cells processed by cryotechniques. Protoplasma 222: 129-37.

Pfeiffer, S., G. Vielhaber, J.P. Vietzke, K.P. Wittern, U. Hintze, and R. Wepf, 2000. High-pressure freezing provides new information on human epidermis: simultaneous protein antigen and lamellar lipid structure preservation. Study on human epidermis by cryoimmobilization. J Invest Dermatol 114: 1030-8.

Pierson, J., U. Ziese, M. Sani, and P.J. Peters, 2011. Exploring vitreous cryo-section-induced compression at the macromolecular level using electron cryo-tomography; 80S yeast ribosomes appear unaffected. J Struct Biol 173: 345-9.

Pinaud, F., S. Clarke, A. Sittner, and M. Dahan, 2010. Probing cellular events, one quantum dot at a time. Nat Methods 7: 275-85.

Polishchuk, R.S., E. San Pietro, A. Di Pentima, S. Tete, and J.S. Bonifacino, 2006. Ultrastructure of long-range transport carriers moving from the trans Golgi network to peripheral endosomes. Traffic 7: 1092-103.

Polishchuk, R.S., E.V. Polishchuk, P. Marra, S. Alberti, R. Buccione, A. Luini, and A.A. Mironov, 2000. Correlative light-electron microscopy reveals the tubular-saccular ultrastructure of carriers operating between Golgi apparatus and plasma membrane. J Cell Biol 148: 45-58.

Porter, K.R., A. Claude, and E.F. Fullam, 1945. A Study of Tissue Culture Cells by Electron Microscopy : Methods and Preliminary Observations. J Exp Med 81: 233-46.

Powell, R.D., C.M. Halsey, and J.F. Hainfeld, 1998. Combined fluorescent and gold immunoprobes: reagents and methods for correlative light and electron microscopy. Microsc Res Tech 42: 2-12.

Prasher, D.C., V.K. Eckenrode, W.W. Ward, F.G. Prendergast, and M.J. Cormier, 1992. Primary structure of the Aequorea victoria green-fluorescent protein. Gene 111: 229-33.

Rigort, A., F.J. Bauerlein, A. Leis, M. Gruska, C. Hoffmann, T. Laugks, U. Bohm, M. Eibauer, H. Gnaegi, W. Baumeister, and J.M. Plitzko, 2010. Micromachining tools and correlative approaches for cellular cryo-electron tomography. J Struct Biol 172: 169-79.

Robinson, J.M., and D.D. Vandre, 1997. Efficient immunocytochemical labeling of leukocyte microtubules with FluoroNanogold: an important tool for correlative microscopy. J Histochem Cytochem 45: 631-42.

Robinson, J.M., and T. Takizawa, 2009. Correlative fluorescence and electron microscopy in tissues: immunocytochemistry. J Microsc 235: 259-72.

Rudner, L., S. Nydegger, L.V. Coren, K. Nagashima, M. Thali, and D.E. Ott, 2005. Dynamic fluorescent imaging of human immunodeficiency virus type 1 gag in live cells by biarsenical labeling. J Virol 79: 4055-65.

Ryman-Rasmussen, J.P., J.E. Riviere, and N.A. Monteiro-Riviere, 2007. Surface coatings determine cytotoxicity and irritation potential of quantum dot nanoparticles in epidermal keratinocytes. J Invest Dermatol 127: 143-53.

Salmon, E.D., and P. Tran, 2003. High-resolution video-enhanced differential interference contrast light microscopy. Methods Cell Biol 72: 289-318.

Sartori, A., R. Gatz, F. Beck, A. Rigort, W. Baumeister, and J.M. Plitzko, 2007. Correlative microscopy: bridging the gap between fluorescence light microscopy and cryo-electron tomography. J Struct Biol 160: 135-45.

Sawada, H., and M. Esaki, 2000. A practical technique to postfix nanogold-immunolabeled specimens with osmium and to embed them in Epon for electron microscopy. J Histochem Cytochem 48: 493-8.

Schikorski, T., 2010. Horseradish peroxidase as a reporter gene and as a cell-organelle-specific marker in correlative light-electron microscopy. Methods Mol Biol 657: 315-27.

Schwartz, H., and B.M. Humbel, 2007. Correlative light and electron microscopy using immunolabeled resin sections, p. 229-256, in: J. Kuo, (Ed.), Electron Microscopy: Methods and Protocols, Humana Press, Totowa NJ.

Seleverstov, O., O. Zabirnyk, M. Zscharnack, L. Bulavina, M. Nowicki, J.M. Heinrich, M. Yezhelyev, F. Emmrich, R. O'Regan, and A. Bader, 2006. Quantum dots for human mesenchymal stem cells labeling. A size-dependent autophagy activation. Nano Lett 6: 2826-32.

Shimomura, O., 2005. The discovery of aequorin and green fluorescent protein. J Microsc 217: 1-15.

Shiurba, R., 2001. Freeze-substitution: origins and applications. Int Rev Cytol 206: 45-96.

Shu, X., V. Lev-Ram, T.J. Deerinck, Y. Qi, E.B. Ramko, M.W. Davidson, Y. Jin, M.H. Ellisman, and R.Y. Tsien, 2011. A genetically encoded tag for correlated light and electron microscopy of intact cells, tissues, and organisms. PLoS Biol 9: e1001041.

Sims, P., R. Albrecht, J.B. Pawley, V. Centonze, T. Deerinck, and J. Hardin, 2006. When Light Microscope Resolution Is Not Enough: Correlational Light Microscopy and Electron Microscopy, in: J. B. Pawley, (Ed.), Handbook of Biological Confocal Microscopy, Springer Science and Business Media, New York.

Sims, P.A., and J.D. Hardin, 2007. Fluorescence-integrated transmission electron microscopy images: integrating fluorescence microscopy with transmission electron microscopy. Methods Mol Biol 369: 291-308.

Slot, J.W., and H.J. Geuze, 2007. Cryosectioning and immunolabeling. Nat Protoc 2: 2480-91.

Small, J., K. Rottner, P. Hahne, and K.I. Anderson, 1999. Visualising the actin cytoskeleton. Microsc Res Tech 47: 3-17.

Sosinsky, G.E., G.M. Gaietta, G. Hand, T.J. Deerinck, A. Han, M. Mackey, S.R. Adams, J. Bouwer, R.Y. Tsien, and M.H. Ellisman, 2003. Tetracysteine genetic tags complexed with biarsenical ligands as a tool for investigating gap junction structure and dynamics. Cell Commun Adhes 10: 181-6.

Spagnuolo, C.C., R.J. Vermeij, and E.A. Jares-Erijman, 2006. Improved photostable FRET-competent biarsenical-tetracysteine probes based on fluorinated fluoresceins. J Am Chem Soc 128: 12040-1.

Spiegelhalter, C., V. Tosch, D. Hentsch, M. Koch, P. Kessler, Y. Schwab, and J. Laporte, 2010. From dynamic live cell imaging to 3D ultrastructure: novel integrated methods for high pressure freezing and correlative light-electron microscopy. PLoS One 5: e9014.

Sternberger, L.A., and N.H. Sternberger, 1986. The unlabeled antibody method: comparison of peroxidase-antiperoxidase with avidin-biotin complex by a new method of quantification. J Histochem Cytochem 34: 599-605.

Steven, A.C., and U. Aebi, 2003. The next ice age: cryo-electron tomography of intact cells. Trends Cell Biol 13: 107-10.

Stewart, W.W., 1981. Lucifer dyes--highly fluorescent dyes for biological tracing. Nature 292: 17-21.

Stroffekova, K., C. Proenza, and K.G. Beam, 2001. The protein-labeling reagent FLASH-EDT2 binds not only to CCXXCC motifs but also non-specifically to endogenous cysteine-rich proteins. Pflugers Arch 442: 859-66.

Sun, M.G., J. Williams, C. Munoz-Pinedo, G.A. Perkins, J.M. Brown, M.H. Ellisman, D.R. Green, and T.G. Frey, 2007. Correlated three-dimensional light and electron microscopy reveals transformation of mitochondria during apoptosis. Nat Cell Biol 9: 1057-65.

Sundara Rajan, S., and T.Q. Vu, 2006. Quantum dots monitor TrkA receptor dynamics in the interior of neural PC12 cells. Nano Lett 6: 2049-59.

Susumu, K., H.T. Uyeda, I.L. Medintz, T. Pons, J.B. Delehanty, and H. Mattoussi, 2007. Enhancing the stability and biological functionalities of quantum dots via compact multifunctional ligands. J Am Chem Soc 129: 13987-96.

Svitkina, T.M., and G.G. Borisy, 1998. Correlative light and electron microscopy of the cytoskeleton of cultured cells. Methods Enzymol 298: 570-92.

Svitkina, T.M., E.A. Bulanova, O.Y. Chaga, D.M. Vignjevic, S. Kojima, J.M. Vasiliev, and G.G. Borisy, 2003. Mechanism of filopodia initiation by reorganization of a dendritic network. J Cell Biol 160: 409-21.

Takizawa, T., and J.M. Robinson, 2003. Ultrathin cryosections: an important tool for immunofluorescence and correlative microscopy. J Histochem Cytochem 51: 707-14.

Takizawa, T., and J.M. Robinson, 2006. Correlative microscopy of ultrathin cryosections in placental research. Methods Mol Med 121: 351-69.

Tokuyasu, K.T., 1973. A technique for ultracryotomy of cell suspensions and tissues. J Cell Biol 57: 551-65.

Trucco, A., R.S. Polishchuk, O. Martella, A. Di Pentima, A. Fusella, D. Di Giandomenico, E. San Pietro, G.V. Beznoussenko, E.V. Polishchuk, M. Baldassarre, R. Buccione, W.J. Geerts, A.J. Koster, K.N. Burger, A.A. Mironov, and A. Luini, 2004. Secretory traffic triggers the formation of tubular continuities across Golgi sub-compartments. Nat Cell Biol 6: 1071-81.

Tsien, R.Y., 2005. Building and breeding molecules to spy on cells and tumors. FEBS Lett 579: 927-32.

Valentijn, J.A., J.H. van Daal, B.G. Jenks, and J.H. van Abeelen, 1989. A method permitting precise trimming of resin-embedded tissue for ultrathin sectioning in pre-embedding immunoelectron microscopy. J Neurosci Methods 30: 55-8.

Valentijn, J.A., K. Valentijn, L.M. Pastore, and J.D. Jamieson, 2000. Actin coating of secretory granules during regulated exocytosis correlates with the release of rab3D. Proc Natl Acad Sci U S A 97: 1091-5.

van Dam, G.J., B.J. Bogitsh, J.A. Fransen, D. Kornelis, R.J. van Zeyl, and A.M. Deelder, 1991. Application of the FITC-anti-FITC-gold system to ultrastructural localization of antigens. J Histochem Cytochem 39: 1725-8.

van Rijnsoever, C., V. Oorschot, and J. Klumperman, 2008. Correlative light-electron microscopy (CLEM) combining live-cell imaging and immunolabeling of ultrathin cryosections. Nat Methods 5: 973-80.

Verdijk, P., R. Dijkman, E.I. Plasmeijer, A.A. Mulder, W.H. Zoutman, A. Mieke Mommaas, and C.P. Tensen, 2005. A lack of Birbeck granules in Langerhans cells is associated with a naturally occurring point mutation in the human Langerin gene. J Invest Dermatol 124: 714-7.

Vetter, J., 1998. Toxins of Amanita phalloides. Toxicon 36: 13-24.

Vicidomini, G., M.C. Gagliani, M. Canfora, K. Cortese, F. Frosi, C. Santangelo, P.P. Di Fiore, P. Boccacci, A. Diaspro, and C. Tacchetti, 2008. High data output and automated 3D correlative light-electron microscopy method. Traffic 9: 1828-38.

Vogels, I.M., K.A. Hoeben, and C.J. Van Noorden, 2009. Rapid combined light and electron microscopy on large frozen biological samples. J Microsc 235: 252-8.

Volkova, E.G., S.Y. Kurchashova, V.Y. Polyakov, and E.V. Sheval, 2010. Self-organization of cellular structures induced by the overexpression of nuclear envelope proteins: a correlative light and electron microscopy study. J Electron Microsc (Tokyo).

Walz, J., A. Erdmann, M. Kania, D. Typke, A.J. Koster, and W. Baumeister, 1998. 26S proteasome structure revealed by three-dimensional electron microscopy. J Struct Biol 121: 19-29.

Wang, Q., C.P. Mercogliano, and J. Lowe, 2011. A ferritin-based label for cellular electron cryotomography. Structure 19: 147-54.

Werner, J.N., E.Y. Chen, J.M. Guberman, A.R. Zippilli, J.J. Irgon, and Z. Gitai, 2009. Quantitative genome-scale analysis of protein localization in an asymmetric bacterium. Proc Natl Acad Sci U S A 106: 7858-63.

Westbroek, W., J. Lambert, P. Bahadoran, R. Busca, M.C. Herteleer, N. Smit, M. Mommaas, R. Ballotti, and J.M. Naeyaert, 2003. Interactions of human Myosin Va isoforms, endogenously expressed in human melanocytes, are tightly regulated by the tail domain. J Invest Dermatol 120: 465-75.

Wilke, K., K. Wick, F.J. Keil, K.P. Wittern, R. Wepf, and S.S. Biel, 2008. A strategy for correlative microscopy of large skin samples: towards a holistic view of axillary skin complexity. Exp Dermatol 17: 73-81.

Wouters, C.H., and H.K. Koerten, 1982. Combined light microscope and scanning electron microscope, a new instrument for cell biology. Cell Biol Int Rep 6: 955-9.

Wulf, E., A. Deboben, F.A. Bautz, H. Faulstich, and T. Wieland, 1979. Fluorescent phallotoxin, a tool for the visualization of cellular actin. Proc Natl Acad Sci U S A 76: 4498-502.

Yoo, J., T. Kambara, K. Gonda, and H. Higuchi, 2008. Intracellular imaging of targeted proteins labeled with quantum dots. Exp Cell Res 314: 3563-9.

Zeuschner, D., W.J. Geerts, E. van Donselaar, B.M. Humbel, J.W. Slot, A.J. Koster, and J. Klumperman, 2006. Immuno-electron tomography of ER exit sites reveals the existence of free COPII-coated transport carriers. Nat Cell Biol 8: 377-83.

Zuber, B., I. Nikonenko, P. Klauser, D. Muller, and J. Dubochet, 2005. The mammalian central nervous synaptic cleft contains a high density of periodically organized complexes. Proc Natl Acad Sci U S A 102: 19192-7.